

# Explainable Deep Learning Methods in Medical Diagnosis: A Survey

CRISTIANO PATRÍCIO and JOÃO C. NEVES, University of Beira Interior, Portugal

LUÍS F. TEIXEIRA, University of Porto, Portugal

The remarkable success of deep learning has prompted interest in its application to medical diagnosis. Even though state-of-the-art deep learning models have achieved human-level accuracy on the classification of different types of medical data, these models are hardly adopted in clinical workflows, mainly due to their lack of interpretability. The black-box-ness of deep learning models has raised the need for devising strategies to explain the decision process of these models, leading to the creation of the topic of eXplainable Artificial Intelligence (XAI). In this context, we provide a thorough survey of XAI applied to medical diagnosis, including visual, textual, and example-based explanation methods. Moreover, this work reviews the existing medical imaging datasets and the existing metrics for evaluating the quality of the explanations. Complementary to most existing surveys, we include a performance comparison among a set of report generation-based methods. Finally, the major challenges in applying XAI to medical imaging are also discussed.

**CCS Concepts:** • Applied computing → Health care information systems.

**Additional Key Words and Phrases:** Explainable AI, Explainability, Interpretability, Deep Learning, Medical Image Analysis

## ACM Reference Format:

Cristiano Patrício, João C. Neves, and Luís F. Teixeira. 2022. Explainable Deep Learning Methods in Medical Diagnosis: A Survey. 1, 1 (May 2022), 36 pages. <https://doi.org/10.1145/nnnnnnn.nnnnnnn>

## 1 INTRODUCTION

The progress made on the last decade in the field of artificial intelligence (AI) has supported a dramatic increase in the accuracy of most computer vision applications. Medical image analysis is one of the applications where the progress made assured human-level accuracy on the classification of different types of medical data (e.g., chest X-rays [80], corneal images [147]). However, and in spite of these advances, automated medical imaging is seldom adopted in clinical practice. According to Zachary Lipton [69], the explanation to this apparent paradox is straightforward, doctors will never trust the decision of an algorithm without understanding its decision process. This fact has raised the need for producing strategies capable of explaining the decision process of AI algorithms, leading subsequently to the creation of a novel research topic named as eXplainable Artificial Intelligence (XAI). According to DARPA [41], XAI aims to “*produce more explainable models, while maintaining a high level of learning performance (prediction accuracy); and enable human users to understand, appropriately, trust, and effectively manage the emerging generation of artificially intelligent partners*”. In spite of its general applicability, XAI is particularly important in high-stake decisions, such as clinical workflow, where the consequences of a wrong decision could lead to human deaths. This is also evidenced by European Union’s General Data Protection Regulation (GDPR) law, which requires an explanation of the decision-making process of the algorithm to make it transparent before it can be used for patientcare [37].

---

Authors’ addresses: Cristiano Patrício, cristiano.patricio@ubi.pt; João C. Neves, jcneves@di.ubi.pt, University of Beira Interior, Covilhã, Portugal, 6201-001; Luís F. Teixeira, luisft@fe.up.pt, University of Porto, Porto, Portugal, 4200-465.

---

Permission to make digital or hard copies of all or part of this work for personal or classroom use is granted without fee provided that copies are not made or distributed for profit or commercial advantage and that copies bear this notice and the full citation on the first page. Copyrights for components of this work owned by others than ACM must be honored. Abstracting with credit is permitted. To copy otherwise, or republish, to post on servers or to redistribute to lists, requires prior specific permission and/or a fee. Request permissions from permissions@acm.org.

© 2022 Association for Computing Machinery.

XXXX-XXXX/2022/5-ART \$15.00

<https://doi.org/10.1145/nnnnnnn.nnnnnnn>

Considering this, it is of utmost importance to invest in the research of novel strategies to improve the interpretability of deep learning methods before being possible to deploy them into clinical practice. During the last years, the research on this topic has focused primarily on devising methods for indirectly analysing the decision process of pre-built models. These methods operate either by analysing the impact of specific regions of the input images on the final prediction (perturbation-based methods [77; 101] and occlusion-based methods [151]) or inspecting the network activations (saliency methods [112; 153]). The fact that these methods can be applied to arbitrary network architectures without requiring an additional customization of the model has supported their popularity in the early days of XAI. However, it has been recently shown that post-hoc strategies suffer from several drawbacks regarding the significance of the explanations [2; 105]. As a consequence, researchers have focused their attention in the design of models/architectures capable of explaining their decision process *per se*. Inherently interpretable models are believed to be particular useful in medical imaging [105], justifying the recent growth in the number of medical imaging works focusing on this paradigm rather than the traditional post-hoc strategies [53; 144]. In spite of the recent popularity of inherently interpretable models, the existing surveys on the interpretability of deep learning applied to medical imaging have not comprehensively review the progress done in this novel research trend. Also, the significant increase in the number of works focused on the interpretation of the decision process of deep learning applied to medical imaging justifies the need for an updated review over the most recent methods not covered by the last surveys on the topic.

To address these concerns, we comprehensively review the recent advances on explainable deep learning applied to medical diagnosis. In particular, this survey provides the following contributions:

- a review of the recent surveys on the topic of interpretable deep learning in medical imaging, including the major conclusions derived from each work, as well as a comparative analysis to our survey.
- an exhaustive list of the datasets commonly used in the study of interpretability of deep learning approaches applied to medical imaging.
- a comprehensive review of the state-of-the-art interpretable medical imaging approaches, covering both post-hoc and inherently interpretable models.
- a complete description of the metrics commonly used for benchmarking interpretability methods either for visual or textual explanations.
- a benchmark of interpretable medical imaging approaches regarding the quality of the textual explanations.
- the future research directions on the topic of interpretable deep learning in medical imaging

## 2 RELATED SURVEYS

Explaining the decisions of deep learning models has been an active area of research, with various methods and algorithms proposed in the literature. The rapid pace of development of XAI has raised the need for comprehensive overviews of the advances over the state-of-the-art, and in most cases, the analysis of specific domains, due to the vast number of works published in the last years. In this section, we provide a critical analysis of the existing surveys in deep learning applied to medical imaging (section 2.1), with a particular focus on explainable approaches (section 2.2). Additionally, we compare the surveys analyzed with our survey (section 2.3).

### 2.1 Deep Learning in Medical Image Analysis

The advent of deep learning significantly changed the field of Computer Vision, where handcrafted feature extraction was replaced by end-to-end learning using Convolutional Neural Networks (CNNs). This new paradigm was fostered by the seminal work of Krizhevsky et al. [58] in 2012, but it was not immediately incorporated by all the applications of Computer Vision. Litjens et al. [71] were the first to review the advances on medical image analysis fostered by the advent of deep learning, where is clear that the use of CNNs in medical imaging research has only become the standard approach in 2017, being clearly preferred over traditional handcrafted

feature extraction for most of the anatomical regions. Based on the works reviewed, the authors concluded that data preprocessing and data augmentation techniques were essential to obtain superior results, and that the combination of medical images with text data (medical reports) could improve the image classification accuracy [110]. Despite the relevance of this survey at the time, the rapid advances in the field of deep learning occurring in the last 5 years have made this work outdated, since the major conclusions of the survey are currently commonsense, and novel deep learning models are being currently used in the medical imaging domain.

Considering this, Rehman et al.[100] provided an updated overview of the advances on deep learning applied to medical image analysis. The survey was divided over the different pattern recognition tasks (image classification, segmentation, image registration). Regarding the image classification task, the authors suggest using generative models to perform data augmentation to improve the results. The survey also gives future research directions to overcome the most common challenges identified by Litjens et al. [71]. The use of techniques such as transfer learning and synthetic data generation were suggested to address these challenges while improving the generalization capability of the developed strategies. Nevertheless, the authors concluded that the non-availability of large-scale annotated datasets remains one of the major challenges in medical imaging, which is impacting the performance of the deep learning models due to the data overfitting and bias issues.

## 2.2 Interpretable Deep Learning in Medical Imaging

The works of Litjens et al. [71] and Rehman et al.[100] show that in the last years the use of deep learning has greatly improved the performance of medical imaging analysis algorithms, allowing also to create a myriad of approaches for the different image modalities and recognition tasks. Nevertheless, this contrasts with the adoption of these algorithms by clinicians who refuse to rely on decisions that they do not understand [69]. In fact, as foresaw by Litjens et al. [71], the importance of designing interpretable models for medical imaging has been growing in the last years and is nowadays one of the major challenges in medical imaging. The following paragraphs describe the different surveys focused on reviewing the recent advances on interpretable deep learning applied to medical imaging. Additionally, the major conclusions derived from each work and a brief comparison to our survey are also outlined.

**2.2.1 General Reviews.** Tjoa and Guan [129] provide a general overview of machine learning and deep learning interpretability methods with emphasis on its application to medical field. The authors consider two types of interpretability: (i) perceptive interpretability, where the saliency methods are included, and (ii) interpretability by mathematical structures, which include some mathematical formulations that can analyze the patterns in data. Although a significant number works per image modality are covered, the survey lacks a comparison between the reviewed works. Also, the survey of Tjoa and Guan is more suitable for technical oriented readers, which is corroborated by a poor intuitive categorization for the medical community. Most works were discussed based on their mathematical foundation instead of describing the rationale behind the proposed method. As major conclusions, Tjoa and Guan state that combining visual and textual explanations is the most promising modality for conveying the explanations of medical imaging analysis algorithms, and that these algorithms should always be considered as a complementary aid/support to clinicians, who should be responsible for the final decision.

Singh et al. [117] propose a review of the works related to the explainability of deep learning models in the context of medical imaging. The methods are broadly divided in two major categories (attribution-based and non attribution-based) with respect to their capability of determining the contribution of an input feature to the target output. Both categories are reviewed by describing works applied to the different image modalities of medical data. Nevertheless, the survey focuses primarily on the attribution-based category, providing a superficial discussion of existing methods on the different categories of non-attribution methods, where inherently interpretable approaches are included. Based on the works reviewed, the authors conclude that leveraging patient record data and images can be an exciting research direction to push forward the performance of deep learning in medical

imaging. When compared to our survey, the work of Singh et al. lacks a comprehensive analysis of inherently interpretable approaches, an analysis of the available medical imaging datasets, and the benchmarking of the most prominent reviewed methods.

Recently, Salahuddin et al. [107] review a set of interpretability methods which are grouped into nine different categories based on the type of explanations generated. They also discuss the problem of evaluating explanations and describe a set of evaluation strategies adopted to quantitative and qualitative measure the explanations' quality. Similar to the other surveys, the authors also emphasize the importance of involving clinicians in designing and validating interpretability models to ensure the utility of the generated explanations. For the future perspectives, Salahuddin et al. claim that case-based and concept-learning models are promising interpretability models for being inherently interpretable and achieving similar performance to black-box CNNs. Despite being one of the most complete surveys on the topic, it lacks the description of most relevant datasets of the field as well as the benchmarking of most prominent approaches reviewed.

**2.2.2 Specific Image Modality Reviews.** In contrast to the above-mentioned works, the work of Pocevičiūtė et al. [97] is focused on a particular image modality. The XAI techniques devised for digital pathology are reviewed with respect to three criteria derived from 1) what is going to be explained (e.g., model predictions, predictions uncertainty); 2) explanation modality; 3) how the explanations are derived (e.g., perturbation-based strategies, interpretable network design). The authors point out the importance of developing a toolbox for objectively measuring the quality of explanations, as the lack of an evaluation framework remains an open problem in the XAI field. Additionally, the authors state that the use of counterfactual examples can enhance the interpretability of the methods. When compared to our survey, this work has disregarded the textual explanation modality, focusing solely on visual explanations, either by visual examples or saliency maps.

Gulum et al. [40] produce a review of the visual explainability techniques applied to cancer detection from Magnetic Resonance Imaging (MRI) scans. Contrary to the work of Pocevičiūtė et al. [97], Gulum et al. discuss the strategies used for measuring the quality of explanations, but they only consider one metric to quantitatively evaluate the explanations. They also emphasize that there is a lack of studies that assess the explanation methods based on human evaluation. As future directions, Gulum et al. highlight the need for developing inherently interpretable approaches, as opposed to the traditional post-hoc strategy. Finally, the authors proposed the use of uncertainty estimation associated with model predictions to perceive how a model is confident in making a prediction. Despite its relevance, the work of Gulum et al. is specific to a particular image modality (MRI) and target disease (cancer).

**2.2.3 Specific Explanation Modality Reviews.** While visual explanations are usually the primary option for explaining the model decisions, these strategies can be unreliable since they often highlight regions regardless of the class of interest [105]. This has fostered the research on textual explanations, and in the particular case of medical imaging led researchers to devise approaches capable of producing different types of textual explanations: 1) textual concepts and 2) textual reports. The recent developments on this topic have been covered in the surveys of Messina et al. [85] and Ayesha et al. [8].

In [85], a thorough overview of the current state-of-the-art on automatic report generation from medical images is provided. The authors review 40 papers with respect to four dimensions: datasets used, model design, explainability and evaluation metrics. Furthermore, a benchmark of most relevant approaches is provided with respect to the performance in terms of NLP metrics on IU Chest X-ray dataset. Based on the works analysed, the authors identify the following challenges and future research directions: 1) the validation of the obtained explanations by clinicians is impractical, being necessary to create automatic metrics positively correlated with the clinicians opinion; 2) most research has concentrated on chest X-rays, mainly due to the availability of public data; 3) supervised learning may not be the most adequate strategy for medical report generation learning, whereas reinforcement learning seems a more reasonable training paradigm to explore.

Similar to the work of Messina et al., Ayesha et al. [8] presents a detailed survey of the existing automatic caption generation methods for medical images. The most used datasets and the evaluation metrics are also discussed. An extensive study is done around the most significant works under the various deep learning-based medical imaging caption generation methods, namely encoder-decoder based, retrieval-based, attention-based, concepts detection-based, and patient's metadata-based. Additionally, a comparative analysis of the performance of the methods reviewed is provided. Finally, Ayesha et al. suggest some future research directions to deal with the main open issues in medical imaging. They point out the lack of large-scale annotated datasets as the major limitation in the medical imaging field, where the data is scarce and often mislabelled. Also, they claim that the lack of a suitable evaluation metric to assess the generated caption remains an open problem since the evaluation of the generated text is based on standard NLP metrics, such as BLEU score, ROUGE, METEOR, and CIDEr. As a final remark, Ayesha et al. also indicate the importance of having a model capable of detecting multiple diseases simultaneously.

### 2.3 Discussion

Despite the significant contributions of each reviewed survey, few of them have described the most important datasets for medical imaging. Moreover, most surveys focused on particular aspects of interpretability, such as visual or textual approaches, and few works have comprehensively reviewed inherently interpretable models devised for medical image analysis. Another problem was the lack of a performance comparison among the reviewed methods. Accordingly, this survey covers these limitations by providing a broader overview of the current state-of-the-art XAI applied to medical diagnosis, including uni and multimodal approaches, followed by the most important medical imaging datasets and a comparative analysis of the models performance using standard evaluation metrics.

Table 1 summarizes the major differences between the reviewed surveys and our work (Ours).

Table 1. Comparative analysis between the surveys on the topic of explainable deep learning applied to medical imaging. Our survey is the first to comprehensively review the advances on the topic regarding the different explanation modalities and the explanation processes. Also, it analyses the most relevant datasets on the field, as well as their use for the development of explainable approaches.

<b>Survey</b>	<b>Year</b>	<b>Explanations</b>		<b>Model Type</b>		<b>Medical Imaging Datasets</b>
		<i>Visual</i>	<i>Textual</i>	<i>Post-hoc</i>	<i>In-model</i>	
Pocevičiūtė et al. [97]	2020	✓	✗	✓	✓	✗
Messina et al. [85]	2020	✗	✓	✗	✓	✓
Tjoa and Guan [129]	2020	✓	✓	✓	✓	✗
Singh et al. [117]	2020	✓	✓	✓	✓	✗
Gulum et al. [40]	2021	✓	✗	✓	✓	✗
Ayesha et al. [8]	2021	✗	✓	✗	✓	✓
Salahuddin et al. [107]	2021	✓	✓	✓	✓	✗
<b>This survey</b>	2022	✓	✓	✓	✓	✓

### 3 BACKGROUND IN XAI

Explainable AI (XAI) is a currently a vibrant and promising research field whose primary purpose is to make the results of AI models more understandable to humans. From a historical perspective, the problem of explaining expert systems has its origin in the mid-80s [88], but the term XAI was only introduced in 2004 by Van et al. [135].

Nevertheless, XAI has only gained prominence when deep learning dominated AI, and the first sign of this interest was demonstrated by the launching, in 2015, of the Explainable AI program by DARPA, whose primary goal was producing more explainable models to increase their understanding and transparency, leading to greater trust by users. Later, the European Union (EU) [37] introduced legislation about the “right to algorithmic explanation” which provided citizens with the right to receive an explanation for algorithmic decisions obtained from personal data. Considering this, researchers shifted their efforts towards the creation of interpretable models rather than simply focusing on accuracy, leading to an exponential increase in the popularity and interest on XAI, whose number of works on the topic has rapidly increased in the last years.

This section provides a general overview of the taxonomy of XAI methods, the description of seminal XAI methods, as well as the existing frameworks providing implementations of these methods.

### 3.1 XAI Methods Taxonomy

Based on the reviewed literature, XAI methods can be categorized according to three criteria: (i) Model-Agnostic versus Model-Specific; (ii) Global Interpretability versus Local Interpretability; and (iii) Post-hoc versus Intrinsic. Figure 1 illustrates the general taxonomy of the XAI methods, and each category is detailed in the following paragraphs.

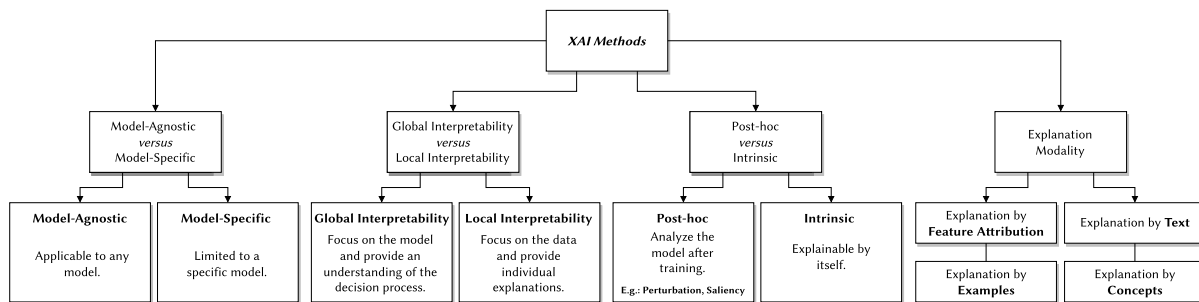


Fig. 1. Categorization of the XAI methods taxonomy.

**Model-Agnostic versus Model-Specific.** A distinguishing factor between interpretability approaches is their comprehensiveness regarding the models that can be applied to. Model-agnostic methods can be used to explain arbitrary models, being not limited to a specific model architecture. Conversely, model-specific methods are restricted to a specific model architecture, meaning that these methods require access to the model’s internal information.

**Global Interpretability versus Local Interpretability.** The type of explanations provided by XAI methods can be broadly divided into global and local whether the explanations provide insights about the model functioning for the general data distribution or for a specific data sample, respectively. Global interpretability methods explain which patterns in the data, i.e., class features, contributed the most to the model’s prediction. These explanations can reveal critical reasoning about what the model is learning. On the other hand, local interpretability methods seek to explain why a model performs a specific prediction for a single input.

**Post-hoc versus Intrinsic.** This criterion distinguishes the methods with respect to whether the explanation mechanism lies in the internal architecture of the model (intrinsic) or if it is applied after the learning/development of the model (post-hoc). Post-hoc methods usually operate by perturbing parts of the data so that they can

understand the contribution of different features in the model prediction, or by analytically determining the contribution of different features to the model prediction. On the other hand, intrinsic models, also known as in-model approaches or inherently interpretable models are self-explainable since they are designed to produce human-understandable representations from the internal model features.

### 3.2 Classical XAI Methods

The first attempts to explain deep learning models relied on the post-hoc analysis of the models. In spite of the criticism that post-hoc approaches have been recently subjected [105], they are still being used in many domains of medical imaging, and their understanding is important to explain the advances on the topic of interpretable deep learning. As such, the following sections briefly describe the most popular XAI algorithms according to the two major categories of post-hoc analysis.

**3.2.1 Perturbation-based methods.** The rationale behind perturbation-based methods is to perceive how a perturbation in the input affects the model's prediction. Two of the most representative perturbation-based methods are LIME [101] and SHAP [77]; and an occlusion-based method [151].

**LIME.** LIME [101] stands for Local Interpretable Model-agnostic Explanations. As the name suggests, it can explain any black-box model, and according to the XAI taxonomy is a post-hoc, model-agnostic method providing local explanations. The intuition behind LIME is to approximate the complex model (black-box model) locally with an interpretable model, usually denoted as local surrogate model. Thus, an individual instance is explained locally using a simple interpretable model around the prediction, such as linear models or decision trees. Figure 2 a) provides an intuitive illustration of the overall functioning of LIME.

In order to approximate the model prediction locally, a new dataset consisting of perturbed samples conditioned on their proximity to the instance being explained is used to fit the interpretable model. The labels for those perturbed samples are obtained through the complex model. In the case of tabular data, the perturbed instances are sampled around the instance being explained, by randomly changing the feature values in order to obtain samples both in the vicinity and far away from the instance being explained. Analogously, when LIME is applied to the image classification problem, the image being explained is first segmented into superpixels, which are groups of pixels in the image sharing common characteristics, such as colour and intensity. Then, the perturbed versions of the original data are obtained by randomly masking out a subset of superpixels, resulting in an image with occluded patches. The new dataset used to fit the interpretable model consists of perturbed versions of the image being explained, and the superpixels with the highest positive coefficients in the interpretable model suggest they largely contributed to the prediction. Thus, they will be selected as part of the interpretable representation that is simply a binary vector indicating the presence or absence of those superpixels.

**SHAP.** SHAP [77] was inspired on the Shapley values from the cooperative game theory [113] and operates by determining the average contribution of a feature value to the model prediction using all combinations of the features powerset. As an example, given the task of predicting the risk of stroke based on age, gender and Body Mass Index (BMI), the SHAP explanations for a particular prediction are given in terms of the contribution of each feature. This contribution is determined from the change observed in model prediction when using the  $2^n$  combinations from the features powerset, where the missing features are replaced by random values. Figure 2 b) illustrates the above-described example. Similar to LIME, SHAP is a local model-agnostic interpretation method that can be applied to both tabular and image data. In the case of tabular data, the explanation is given in the form of importance values to each feature. In the case of image data, it follows a similar procedure to the LIME, by calculating the Shapley values for all possible combinations between superpixels. Several variations of SHAP method were proposed to approximate Shapley values in a more efficient way, namely KernelSHAP, DeepSHAP and TreeSHAP [76].

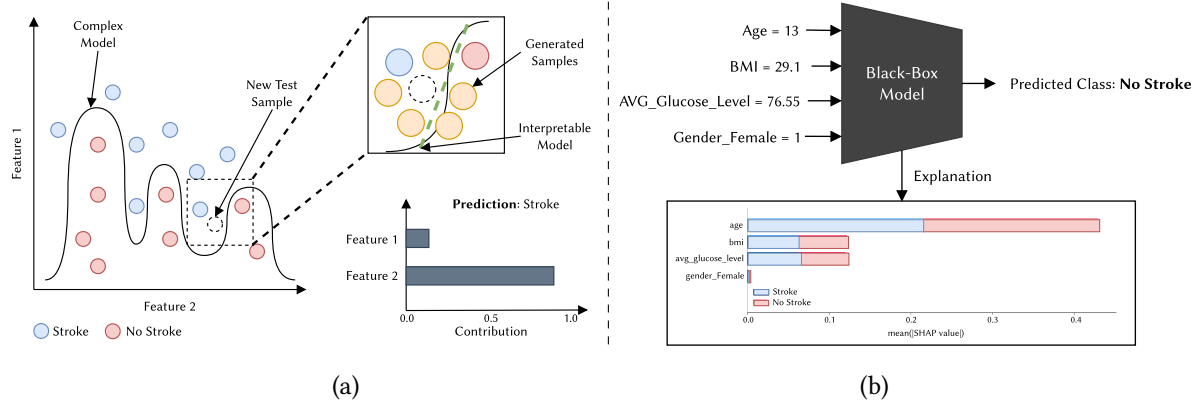


Fig. 2. (a) **LIME**. The black curved line represents decision boundary learned by the complex black-box model. LIME explains a new test sample (dashed circle), by fitting an interpretable model (represented by a green dashed line) to the variations of the test sample (orange circles), which are generated by randomly perturbing the test sample features. The fitted model allows to perceive the contribution of each feature for classifying that specific test sample. (b) **SHAP**. The predicted risk of stroke of a classification model for a female person with 13 years, a body mass index of 29.1 and an average glucose level of 76.55 was “No Stroke”. As evidenced by the bar plot, which provides the Shapley values for each feature, “age” was the feature with a higher impact on the prediction of “No Stroke”, followed by the BMI and average glucose level features.

**3.2.2 Saliency.** Saliency maps are one of the most popular techniques to explain the decisions of a model. Saliency methods produce visual explanation maps representing the importance of image pixels to the model classification.

Class Activation Mapping (CAM) [153] is a seminal saliency method which allowed the generation of a saliency map using a linear combination of the output of the last Global Average Pooling (GAP) layer of the network. Despite being a seminal contribution, CAM can only be applied to architectures following a specific pattern: convolutional layers, followed by a GAP layer connected to a single fully-connected layer. To address this problem, Selvaraju et al. [112] proposed the Gradient-weighted Class Activation Mapping (Grad-CAM) [112] that uses the gradient information of the target class with respect to the input image to produce a class-discriminative localization map that act as a visual explanation for the model’s prediction. Grad-CAM is a generalization of CAM. The main difference between Grad-CAM and CAM is that the latter requires a particular kind of CNN architecture. Alternatively, SmoothGrad [122] is another gradient-based explanation method whose core idea is to attenuate the noise of the explanations provided by other gradient-based techniques. The rationale behind SmoothGrad is to sample multiple images from the input image by adding noise to it. Then, the sensitivity maps are computed for each sampled image. The final map is the average of the sensitivity maps.

The Integrated Gradients (IG) [127] is an attribution method that relies on generating a set of images between the baseline and the original image using linear interpolation. These interpolated images are minor changes in the feature space between the baseline and input image and consistently increase with each interpolated image’s intensity. Calculating the gradients per feature (pixels) makes it possible to measure the correlation between changes to a feature and changes in the model’s predictions. The pixels with a high score are the ones that contributed the most to the prediction. The Layer-wise Relevance Propagation (LRP) [9] is an alternative solution to the use gradients, where the decision function is decomposed into the relevance score of neuron in the network. The output is propagated backwards through the model to determine the relevance score of the input, allowing to produce an importance heatmap of image pixels.

The main advantage of saliency methods is the reduced computational cost when compared to perturbation-based methods. However, different studies argue that the explanations provided by gradient-based methods can be ambiguous and unreliable, as well as sensitive to adversarial perturbations [2; 35].

### 3.3 Interpretability Frameworks

The increasing interest in the interpretability of machine learning fostered the development of frameworks implementing classical XAI methods. The LRP Toolbox [62] was launched in 2016 and provides the implementation of the LRP [9] algorithm for artificial neural networks supporting Matlab and Python. Additionally, the LRP toolbox released an extension to be compatible with the Caffe Deep Learning framework. DeepExplain [6] is a framework that implements perturbation and gradient-based attribution methods, including Saliency Maps [116], Gradient \* Input [114], Integrated Gradients (IG) [127], DeepLIFT [114],  $\epsilon$ -LRP [9], and DeConvNet [151]. It also supports Tensorflow as well as Keras with Tensorflow backend. Alternatively, iNNvestigate [4] is a more complete toolbox that provides implementations for SmoothGrad [122], DeConvNet [151], Guided-BackProp [125], PatternNet [55], Input \* Gradients [114], DeepTaylor [87], PatternAttribution [55], LRP [9] and Integrated Gradients (IG) [127]. It also supports Tensorflow and Keras.

With regard to PyTorch frameworks, TorchRay [32] implements several visualization methods, namely Gradient [116], Guided-BackProp [125], Grad-CAM [112] and RISE [96]. TorchRay is considered research-oriented, since it provides code for reproducing results that appear in several papers. Captum [57] is a PyTorch library that provides state-of-the-art algorithms for model interpretability and understanding. It contains general purpose implementations of Integrated Gradients, Saliency maps, SmoothGrad, VarGrad and others for PyTorch models. Table 2 summarizes the aforementioned frameworks alongside the supported XAI methods. Additionally, we refer the author to the work of Darias et al. [25] in which some other model-agnostic XAI libraries were approached.

Table 2. Publicly available interpretability frameworks.

Framework	Year	Methods
LRP Toolbox [62]	2016	LRP
DeepExplain [6]	2017	Saliency maps, Grad * Input, $\epsilon$ -LRP, DeepLIFT, DeConvNet
iNNvestigate [4]	2019	SmoothGrad, DeConvNet, Guided-BackProp, PatternNet, LRP Input * Gradients, DeepTaylor, PatternAttribution, IG
TorchRay [32]	2019	Gradient, Guided-BackProp, Grad-CAM, RISE
Captum [57]	2019	SmoothGrad, DeConvNet, Guided-BackProp, PatternNet, LRP Input * Gradients, DeepLIFT, DeepTaylor, LIME, Kernel SHAP, IG

## 4 DATASETS

Among the reviewed literature, a set of 23 publicly available medical imaging datasets were considered to provide a thorough overview of the existing medical imaging databases. Table 5 presents the main characteristics of the selected datasets, grouped by image type.

### 4.1 Chest X-ray

With respect to X-ray imaging modality, IU Chest X-ray [27], Chest X-ray 14 [142], CheXpert [47], MIMIC-CXR [49], PadChest [16], COVIDx [139], and VinDr-CXR [91] datasets pertain to the chest anatomical region.

Moreover, IU Chest X-Ray, MIMIC-CXR, and PadChest datasets include free-text radiology reports. The reports are written in English, except for the PadChest dataset, whose reports are written in Spanish. MIMIC-CXR and CheXpert are the largest databases, composed by 377, 110 and 224, 316 radiographs, respectively. CheXpert does not provide the raw free-text reports, but it provides an automated rule-based labeller for extracting keywords from medical reports conforming to the Fleischner Society's recommended glossary [43]. This tool was also used in the MIMIC-CXR dataset to extract the labels from the radiology reports. UI Chest X-Ray [27] comprises 7, 470 chest X-ray images jointly with 3, 955 free-text reports, being the most used dataset in the literature. The VineDr-CXR consists of 18, 000 chest X-ray images annotated with 22 findings (local labels) and 6 diagnosis (global labels). The local labels are inferred from the "findings" section in the radiology reports. In contrast, the global labels come from "impressions" section and indicate suspected diseases, such as "Pneumonia", "Tuberculosis", "Lung Tumor", "Chronic obstructive pulmonary disease", "Other diseases", and "No Findings". Additionally, each "finding" is annotated on the X-ray image with a bounding box. Finally, COVIDx [139] dataset comprises 13,975 chest x-ray images across 13, 870 patient cases, distributed by "Normal", "Pneumonia" and "COVID-19" cases.

It is worth noting that the majority of the chest X-ray dataset's labels were extracted using an automatic rule-based labeler, such as the CheXpert NLP tool [47]. However, relying on these automated tools can pose several issues concerning the quality of the labels. Consequently, the authors of the VinDr-CXR [91] dataset provided only radiologist-level annotations in both training and test sets.

#### 4.2 Other X-ray

In the same segment of the X-ray imaging, and similar to the VinDr-CXR [91] dataset approach, VinDr-SpinalXR [92] is a recent dataset comprising 10, 469 spine X-ray images manually annotated by an experienced radiologist with bounding-boxes around abnormal findings in 13 categories. The Knee Osteoarthritis [90] dataset contains 8,894 knee X-rays for both knee joint detection and knee Kellgren and Lawrence grading [51], whose value ranges from 0 to 4, according to the level of severity. Regarding the mammography datasets, Inbreast [89] consists of 410 mammography x-rays along with 115 radiology reports written in Portuguese. Similarly, CBIS-DDSM [65] dataset is composed of 2, 620 mammography scans distributed into "Normal", "Benign", and "Malignant" cases.

#### 4.3 Dermatoscopy

In the scope of dermatology, the ISIC 2020 [104] dataset consists of 33, 126 skin lesion images of different categorizations (malignant, melanoma, keratosis, etc), and it is part of the International Skin Imaging Collaboration, which promotes annual challenges to enhance the diagnosis of malignant skin lesions in dermoscopy images. The HAM10000 [132] dataset consists of 10, 015 dermatoscopic images distributed into diagnostic categories in the realm of pigmented lesions. The PH<sup>2</sup> [84] dataset comprises 200 dermatoscopic images of melanocytic lesions, including common nevi, atypical nevi, and melanoma. Moreover, the PH<sup>2</sup> database includes medical segmentation of the lesions, clinical and histological diagnosis, and the assessment of several dermatoscopic criteria. The Derm7pt [50] is another dermatoscopic image dataset with over 2, 000 images annotated following the 7-point melanoma checklist criteria. Finally, the SKINL2 [26] database consists of a total of 376 light fields of skin lesions manually annotated under eight categories, based on the type of skin lesion and using the correspondent International Classification of Diseases (ICD) code.

#### 4.4 Microscopy

With regard to datasets composed of microscopy images, the BreakHis [124] dataset comprises 9, 109 microscopic images of breast tumour tissue distributed in various magnifying factors (40x, 100x, 200x, and 400x) and categorized into "benign" and "malignant" tumours. The Camelyon 17 [70] dataset consists of 1, 000 annotated whole-slide images (WSI) of lymph nodes. It is part of a challenge whose primary goal is the classification of breast

cancer metastases in WSI of histological lymph node sections. Similarly, Databiox [15] dataset comprises 922 histopathological microscopy images with four levels of magnification (4x, 10x, 20x, and 40x) for the task of Invasive Ductal Carcinoma (IDC) grading using three grades of IDC.

#### 4.5 Others

For blindness detections purposes, the APTOS [123] dataset provides 5,590 images of the retina taken using fundus photography. A clinician annotated each image according to the severity of diabetic retinopathy on a scale of 0 (Diabetic Retinopathy) to 4 (Proliferative Diabetic Retinopathy).

Regarding databases with multiple imaging modalities, the Pathology Education Informational Resource (PEIR) is a multidisciplinary public access image database intended for medical education. The PEIR database consists of 33,648 images and the respective descriptions from different sub-classes of PEIR albums (PEIR Pathology, PEIR Radiology, and PEIR Slice). Similarly, the Radiology Objects in COntext (ROCO) [95] dataset is a multimodal image dataset consisting of 81,825 radiology images divided into CT, MRI, X-ray Ultrasound, and Mammography. Each image is accompanied by the corresponding caption and the annotated Unified Medical Language System (UMLS) concepts.

#### 4.6 Discussion

In short, and as denoted by the imaging modalities (“Image Type” column) presented in table 3, Chest X-ray is the prevalent imaging modality and also the one that gathers the large-scale databases, namely MIMIC-CXR and CheXpert. On the other hand, as evidenced by the number of images per dataset, the scarcity of large-scale datasets concerning other imaging modalities is noticed.

### 5 XAI METHODS IN MEDICAL DIAGNOSIS

As aforementioned, deep learning models must confer transparency and trustworthiness when deployed in real-world scenarios. Moreover, this requirement becomes particularly relevant in clinical practice, where a less informed decision can put patient’s lives at risk. Among the reviewed literature, several methods have been proposed to confer interpretability in the deep learning methods applied to medical diagnosis. The following sections summarize and categorize the most relevant works in the scope of explainable models applied to medical diagnosis. Furthermore, we give particular attention to the inherently interpretable neural networks and their applicability to medical imaging. We categorize the methods according to the explanation modality: (i) Explanation by Feature Attribution, (ii) Explanation by Text, (iii) Explanation by Examples, (iv) Explanation by Concepts, and (v) Other Approaches; inspired by the taxonomy presented in [86]. The list of the reviewed methods categorized by the algorithm used, image modality, and the dataset is provided in Table 4.

#### 5.1 Explanation by Feature Attribution

Feature attribution methods indicate how much each input feature contributed to the final model prediction. These methods can work on tabular data or image data by depicting feature importance scores in a bar chart or using a saliency map, respectively. Among the existing feature attribution approaches in the literature, we categorize them into (i) perturbation-based methods and (ii) gradient-based methods, emphasizing their application to medical image analysis. A schematic diagram illustrating the general pipeline of these methods is shown in Figure 3.

**5.1.1 Perturbation-based methods.** As previously described in section 3.2.1, perturbation-based methods aim to perform a modification in the input data to perceive how it affects the model’s prediction. Popular examples of perturbation-based methods are LIME [101] and SHAP [77]. Regarding the use of perturbation methods to explain the prediction medical diagnosis algorithms, Malhi et al. [81] applied the LIME method to explain the

Table 3. Medical Imaging Datasets. The datasets marked with a “\*\*” mean that the given reports are written in Spanish. Conversely, the datasets marked with a “\*\*\*” mean that the reports are written in Portuguese.

Dataset	Image Type	Year	No. Images	Notes
IU Chest X-Ray [27]	Chest X-ray	2016	7,470	Includes reports
Chest X-Ray14 [142]	Chest X-ray	2017	112,120	Multiple labels
CheXpert [47]	Chest X-ray	2019	224,316	Multiple labels
MIMIC-CXR [49]	Chest X-ray	2019	377,110	Includes reports
PadChest* [16]	Chest X-ray	2020	160,868	Includes reports
VinDr-CXR [91]	Chest X-ray	2020	18,000	Multiple labels
COVIDx [139]	Chest X-ray	2020	13,975	Multiclass
Inbreast** [89]	Mammography X-ray	2012	410	Includes reports
CBIS-DDSM [65]	Mammography X-ray	2017	2,620	Multiclass
VinDr-SpineXR [92]	Spinal X-ray	2021	10,469	Multiple labels/BBox
Knee Osteoarthirtis [90]	Knee X-ray	2006	8,894	Multiclass
PH <sup>2</sup> [84]	Dermatoscopic Images	2013	200	Multiple labels/Lesion segment.
HAM10000 [132]	Dermatoscopic Images	2018	10,015	Multiclass
SKINL2 [26]	Dermatoscopic Images	2019	376	Multiclass
Derm7pt [50]	Dermatoscopic Images	2019	2,000	Multiclass
ISIC 2020 [104]	Dermatoscopic Images	2020	33,126	Multiple labels
BreakHis [124]	Microscopy Images	2015	9,109	Multiclass
Camelyon17 [70]	Microscopy Images	2018	1,000	Multiclass
Databiox [15]	Microscopy Images	2020	922	Multiclass
BCIDR( <sup>priv</sup> ) [152]	Microscopy Images	2017	5,000	Includes reports
APTOPS [123]	Retina Images	2019	5,590	Multiclass
LIDC-IDRI [7]	CT scans	2011	1,018	Includes annotations
PEIR [48]	Photographs	2017	33,648	Includes reports
ROCO [95]	Multimodal	2018	81,825	Includes reports/UMLS Concepts

decisions of a classifier to detect bleeding in gastral endoscopy images. Similarly, Punn et al. [98] applied the LIME technique to explain the predictions of various state-of-the-art deep learning models used to classify pulmonary diseases in chest x-ray images. Magesh et al. [79] also used LIME to justify the decisions of a Parkison’s disease classifier model. In the context of melanoma detection, Young et al. [149] used Kernel SHAP [77] interpretability method to investigate its reliability in providing explanations for a melanoma classifier from dermoscopy images. They concluded that the interpretability strategy highlighted irrelevant features to the final prediction. The authors also conducted sanity checks on the interpretability methods, which confirmed that these methods often produce different explanations for models with similar performance. This can be explained by the fact that the model can learn some spurious correlations, causing interpretability methods to give exaggerated importance to those spurious regions highlighted on the produced saliency maps. In the same context, Wang et al. [141] proposed a multimodal CNN for skin lesion diagnosis, which considered patient metadata and the skin lesion images. To analyze the contribution of each feature regarding the patient metadata, they adopted SHAP. Similarly,

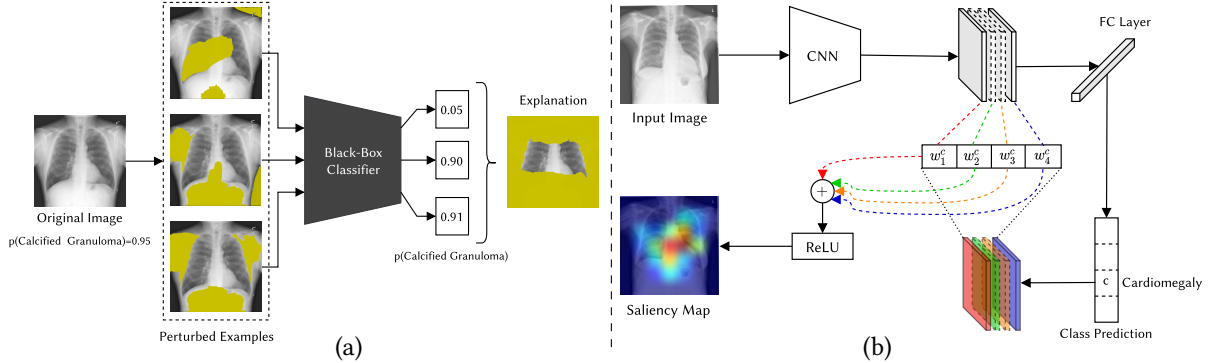


**Fig. 3. (a) Perturbation-based methods.** The input image is randomly perturbed by turning on and off certain pixels, resulting in an image with occluded parts (*Perturbed Examples* in the figure). Then, the perturbed image is fed to the classification model and the prediction confidence is exploited to determine the regions that contributed positively to the class prediction. Therefore, those regions will be considered to obtain the final explanation map (*Explanation* in the figure). **(b) Gradient-based methods.** The input image is fed to the classification model to obtain a class prediction. Then, the gradient is calculated for the score of the class concerning the feature maps of the last convolutional layer. After calculating the importance of the feature map regarding the predicted class, they are weighted with each of respective weight, followed by a ReLU operation to obtain the final saliency map.

Eitel et al. [30] relied on an occlusion-based interpretability method [151] and investigated its robustness for the task of Alzheimer’s disease classification. RISE was proposed by Petsiuk et al. [96], consisting of a post-hoc model-agnostic method for explaining the predictions of a black-box model through the generation of a saliency map indicating the important pixels to the model’s prediction. The core idea is to probe the model with a set of perturbed images from the input image via random masking to perceive the model’s response as important regions of the image are randomly occluded. The final saliency map is generated as a linear combination of the generated masks weighted with the output probabilities predicted by the model. For evaluation, the authors proposed two novel metrics, namely deletion and insertion, based on the removal and insertion of important pixels in the image to perceive the increase or the decrease of the model’s performance.

**5.1.2 Saliency Methods.** Saliency methods allow to produce a saliency map in which each pixel is assigned with a value that represents its relevance to the prediction of a certain class. Popular techniques are CAM [153], Grad-CAM [112], DeepLIFT [114] and Integrated Gradients [127].

Rajpurkar et al. [99] proposed the CheXNeXt model to detect pulmonary pathologies and used CAM to identify the locations on the chest radiograph that contributed most to the final model prediction.

In the context of detecting COVID-19 from chest radiographs, Lin et al. [68] used Grad-CAM and Guided Grad-CAM to investigate the regions where the CNN model was focused for classification. The produced heatmaps showed that when no preprocessing is used, the CNN tends to concentrate on non-lung areas (e.g., spine, heart, background), deemed irrelevant for the classification decision. However, when a masking process is used to salient only the lung’s area, the produced heatmaps highlight only the relevant regions since the CNN attention is limited to the critical area for detecting pulmonary diseases (lung’s area). Following the same procedures, Lopatina et al. [73] used DeepLIFT attribution algorithm to investigate the decisions of a multiple sclerosis classification model, and Sayres et al. [109] used Integrated Gradients to provide explanations for the task of predicting diabetic retinopathy from retinal fundus images.

In contrast to the previous approaches, Rio-Torto et al. [102] proposed an in-model joint architecture composed of an explainer and a classifier to produce visual explanations for the predicted class labels. The explainer consists of an encoder-decoder network based on U-Net, and the classifier is based on VGG-16. Since the classifier is trained using the explanations provided by the explainer, the classifier focuses only on the relevant regions of the image containing the class. To qualitatively assess the provided explanations, the authors employed some state-of-the-art explainability methods included in the Captum library [57].

*Discussion.* Despite the simplicity of the feature attribution methods and their applicability to a wide range of approaches, these methods may often produce ambiguous explanations, difficulting their qualitative evaluation. Furthermore, preprocessing techniques were required for some methods to generate more plausible explanations [68]. Thus, researchers began exploring other modalities, such as textual explanations, and it was discovered that textual explanations were indeed valid explanations and, in some cases, preferred over visual explanations since they are inherently understandable by humans [138].

## 5.2 Explanation by Text

The use of semantic descriptions became another way of providing explanations to the model decisions since most of the clinicians prefer textual explanations compared to visual explanations solely, and the combination of textual and visual explanations over either alone [34]. In general, providing textual explanations can be built on three paradigms: (i) image captioning, (ii) image captioning with visual explanation, and (iii) concept attribution [138]. Figure 4 depicts the general scheme adopted by most of works to generate a textual description based on the visual features of the input image.

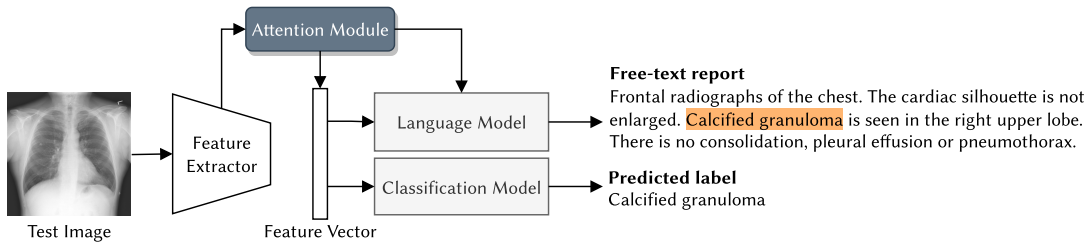


**Fig. 4. Explanation by textual descriptions.** The typical architecture for obtaining a textual description from image data is based on an image embedding model (e.g., CNN) to extract the features from the input image and a language model (e.g., LSTM) to generate the word sentences. The attention module can be inserted between those two models to guide the language model to focus only on relevant regions of the input image to improve the generation of the word sentences.

The task of generating a textual description capable of explaining a model decision can be viewed as an image captioning problem, commonly treated in Natural Language Processing (NLP). Moreover, the vast majority of works that aim to generate a textual description for a given input image relied on a CNN for extracting the visual features followed by an RNN (e.g., LSTM) to generate the word sentences. Based on this paradigm, Sun et al. [126] developed a joint framework relying on a CNN and a RNN to generate sequences of words to provide a textual explanation for the task of diagnosing malignant tumors from breast mammography. Similarly, Singh et al. [120] built on an encoder-decoder framework composed of a CNN and a stacked Long Short-Term Memory (LSTM) for automatically generating radiology reports from chest X-rays. Regarding image captioning with visual explanation, Zhang et al. [152] proposed a multimodal approach, dubbed MDNet, composed of an image embedding model and a language model, that can generate diagnostic reports, retrieve images by symptom descriptions, and visualize network attention. The MDNet model was evaluated on a dataset (BCIDR) containing

histopathological images of bladder cancer. Furthermore, MDNet inspired several approaches. For example, Jing et al. [48] proposed a multi-task learning framework with a co-attention mechanism to guide the generation of text according to the localized regions containing abnormalities. They showed that a hierarchical LSTM model performs better in generating long text reports. Subsequently, Wang et al. [143] proposed TieNet, which makes use of attention modules to extract the most important information from chest X-ray images and also use their diagnostic reports in order to guide the model to produce more coherent reports. Similarly, Barata et al. [11] proposed a hierarchical classification model that uses attention modules, including channel and spatial attention, to identify relevant regions in the skin lesions and subsequently guide further the LSTM attending at different locations whilst conferring more transparency to the network. Lee et al. [64] also explained the decisions of a breast masses classifier using both visual and textual explanations, based on a CNN-RNN architecture. In the same fashion, Gale et al. [34] proposed a model-agnostic interpretable method based on a RNN to produce textual explanations for the decisions of deep learning classifiers. Furthermore, Gale et al. [34] developed a visual attention mechanism in charge of highlighting the relevant regions for classifying hip fractures in pelvic X-rays. Yin et al. [148] also used attention mechanisms to attend to the regions at sentence level. They proposed the Hierarchical Recurrent Neural Network (HRNN) model, composed of two-level LSTMs: a word RNN and a sentence RNN. The sentence RNN produces the topic vectors. The word RNN receives the output of the sentence RNN and infer the words that constitute the final report. Moreover, they introduced a matching mechanism to map the topic vectors and the sentences into a jointly semantic space that minimizes a contrastive loss. Similar to the work of Yin et al. [148], the model proposed by Liu et al. [72] generates topics from images and then complete sentences from these topics. When compared to [148], this work allows the generation of more coherent report generation due to the use of a fine-tuning process that uses reinforcement learning via CIDEr.

A more disruptive approach was introduced by Li et al. [66] that proposed the Hybrid Retrieval-Generation Reinforced Agent (HRGR-Agent) consisting of a retrieval policy module and a generation module. The retrieval policy module is responsible for deciding whether sentences are obtained from a generation module or retrieved from the template database, which is composed of a set of template sentences. Moreover, the retrieval policy and generation modules are updated via reinforcement learning, guided by sentence-level and word-level rewards using the CIDEr.

In contrast to the previous approaches, Chen et al. [21] exploited the Transformer [136] architecture, where they incorporated two memory modules into the decoder. These modules are responsible for memorizing textual patterns and assisting the decoder of the Transformer in generating radiology reports containing relevant information associated with chest X-ray images.

**5.2.1 Concept Attribution.** The idea behind concept-based attribution is learning human-defined concepts from the internal activations of a CNN. The use of concepts to provide global explanations was proposed by Kim et al. [52] with the introduction of the Concept Activation Vectors (CAVs), which provide explanations in terms of human-understandable concepts that are typically related to parts of the image. Kim et al. also proposed Testing with CAVs (TCAV), which enable to quantify the importance of a user-defined concept to a classification result. Figure 5 illustrates the typical pipeline of concept-based attribution methods. In the context of medical imaging, the term “microaneurysm” can be viewed as a concept, being possible to be identified by humans in fundus imaging, and which denote the presence of diabetic retinopathy [138]. In the same line of research, Graziani et al. [39] proposed a framework for concept-based attribution to generate explanations for CNN decisions of a breast histopathology classifier. They built on TCAV by incorporating Regression Concept Vectors (RCV), which provide continuous-values measures of a concept instead of solely indicating its presence or absence (TCAV). This is particularly useful in the medical domain since a value indicating, for example, tumour size is more informative than a binary value indicating its presence or absence. Graziani et al. also concluded that the learning of concepts by an intermediate layer of a CNN could be improved by removing spatial dependencies of

the convolutional layers and introducing L2 norm regularization in the regression problem. Recently, Lucieri et al. [74] introduced ExAID, a framework that provides multimodal concept-based explanations for the task of melanoma classification. Their framework relied on CAVs for concept identification and used the TCAV method to estimate the influence of a specific concept on the decision. Having the relevant concepts identified and their importance score given by the TCAV, the authors provided textual explanations in the form of template phrases by only replacing the identified concepts and their importance to the prediction in the phrase structure. In order to localize the regions of the learned concepts in the latent space of the trained classifier, the authors used the Concept Localization Maps [75] which uses perturbation-based concept localization to generate a saliency map highlighting the relevant regions with respect to the learned concepts, thus providing visual explanations.

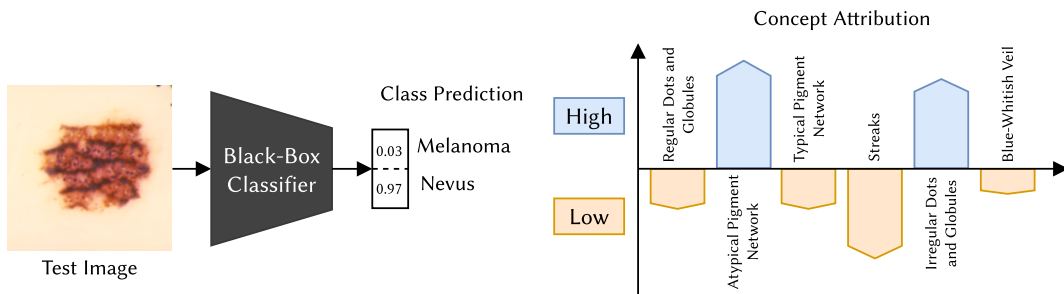


**Fig. 5. Explanation by concept attribution.** In the first phase, the human-defined concepts (Regular Dots and Globules, Atypical Pigment Network, Typical Pigment Network, Streaks, Irregular Dots and Globules, and Blue-Whitish Veil) are modelled as numeric features, following the CAV technique. Then, after the input image passes through a classifier model, the class prediction is globally explained based on the computed relevance importance scores for each defined concept, denoting the importance of each concept to the final prediction.

**Discussion.** In summary, except for the work of Chen et al. [21], all the explanation text-based approaches mentioned above relied on RNN architectures to generate text descriptions towards providing a more human-interpretable explanation for a model decision. However, as stated by Pascanu et al. [94], RNN-based approaches, such as LSTM, have some limitations in generating long text reports. On the contrary, concept-based attribution methods provide a more objective and human-understandable way of interpreting classification decisions. However, the main limitation of these methods is the need for manual annotations of the concept examples, which may be impractical for specific medical image modalities, increasing the need for involving clinicians in the annotation tasks.

### 5.3 Explanation by Examples

The type of methods that explain a model decision by selecting a set of similar examples are dubbed example-based explanation methods. Apart from explaining algorithm decisions, this strategy is also commonly used between clinicians to explain the rationale behind their decision process. Below, we categorize example-based explanation methods into the following categories: (i) Case-Based Reasoning, (ii) Counterfactual Explanations, and (iii) Prototypes.

**5.3.1 Case-Based Reasoning.** Case-Based Reasoning (CBR) and Content-Based Image Retrieval (CBIR) are example-based explanation methods that aim to search a database for visually similar entries to a specific query image.

The general scheme for implementing a CBR system using DNNs is depicted in Figure 6. Although the idea of using CBIR systems in clinical settings is not novel [3], there has been renewed interest in CBIR approaches as a way to provide explainability to deep learning methods for medical diagnosis [5; 22; 42].

Recently, Barnett et al. [13] introduced a novel interpretable AI algorithm (IAIA-BL) for classifying breast masses using CBR. The model provided both a prediction of malignancy and its explanation by using known medical features (mass margins). Given an image region to analyze, the algorithm compared that region with a set of previous similar cases (image patches) using L2 distance. The similarity score was then used to provide the mass margin scores for each medical feature, and those scores were then used to predict the malignancy score (benign or malignant). The model was trained using a fine-annotation loss that penalizes activations of medically irrelevant regions on the data with fine-annotations. The authors also introduced an interpretable evaluation metric, namely Activation Precision, to quantify the proportion of relevant information from the “relevant region” used to classify the mass margin regarding the radiologist annotations. The experimental results showed that the IAIA-BL achieved comparable performance to black-box models, namely VGG-16.

A different approach was presented in the work of Tschandl et al. [131], in which they compared the predictions of the ResNet-50 softmax classifier with the diagnostic accuracy obtained by using CBIR. Contrary to Barnett et al. [13], Tschandl et al. measured the cosine similarity between two feature vectors to retrieve the most similar images to the image query. The results showed that the diagnostic accuracy obtained through CBIR is comparable to the performance of using a softmax classifier. Furthermore, Tschandl et al. claimed that CBIR might be more helpful than softmax classifiers in improving clinician’s diagnostic accuracy in a clinical workflow.

A more recent approach was introduced by Barata and Santiago [12], where CBIR was applied to explain the decisions of a Deep Neural Network (DNN) model for skin cancer diagnosis. When compared to the work of Tschandl et al., Barata and Santiago implemented an augmented category-cross entropy loss function composed of three regularization losses, namely the triplet loss, the contrastive loss, and the distillation loss. These losses encourage the model to learn a more structured feature space. Thus, the final model is able to classify the dermoscopy images and provide justifications through retrieved similar images. The experimental results on ISIC 2018 [132] dermoscopy dataset confirmed that the combination of different loss functions lead to more structured feature spaces, which improves the performance of the classification model. Lamy et al. [61] proposed an explainable CBR system with a visual interface, combining quantitative and qualitative approaches. In contrast to the above-discussed works, it used numerical data and provided a user study in which clinicians validated their approach.

The recent work of Hu et al. [46] introduced the eXplainable Medical Image Retrieval (X-MIR) approach, which explored the use of similarity-based saliency maps to explain the retrieved images visually. Concretely, they adapted the saliency map generation process for the problem of image retrieval through the use of a similarity-based formulation. These similarity-based saliency methods take as input a retrieval image and a query image for producing a saliency map highlighting the most similar regions of the retrieval image to the query image. To evaluate the quality of the generated saliency maps, the authors adapted two causal metrics, namely deletion and insertion (refer to section 6.1 for a detailed description), to measure the decrease or increase in image similarity score as the retrieved image is gradually perturbed based on the important regions of its saliency map. The authors evaluated their approach on two medical datasets, namely COVIDx [139] and ISIC 2017. They found that for both cases, the generated saliency maps focused on relevant regions when retrieved images were correct and observed the contrary when the retrieved images were incorrect. Finally, the authors pointed out for the importance of conducting user studies with clinicians to validate the utility of their approach. Silva et al. [115] also explored the medical image retrieval with the addition of saliency maps to improve the class-consistency of top retrieved results while enhancing the interpretability of the whole system by accompanying the retrieval with visual explanations.

In order to assess the effectiveness of using a CBIR system as an auxiliary tool for classifying skin lesions through dermatology images, a user-centered study was done by Sadeghi et al. [106]. They invited 16 non-expert users to classify skin lesions images among four categories (Nevus, Seborrheic Keratosis, Basal Cell Carcinoma, and Malignant Melanoma) based on two conditions: using CBIR and without using CBIR. The results indicated that CBIR enabled users to make a significantly more accurate classification on a new skin lesion image. These findings suggest that CBIR can indeed assist clinicians understand model decisions as well as allow less experienced practitioners to improve their skills. Thus, CBIR-based systems can have a significant clinical application value as a decision-support tool to accelerate the diagnosis of pathologies.

**5.3.2 Counterfactual Explanations.** Counterfactual explanations are based on the principle that “an action on the input data will cause an outcome” [86]. The idea is to perturb the input data in a controlled way in order to reverse the final model prediction, being the modified input the counterfactual example, as illustrated in the diagram of the Figure 6b). Furthermore, counterfactual explanations are deemed human-interpretable and post-hoc, meaning that they do not require access to model internals.

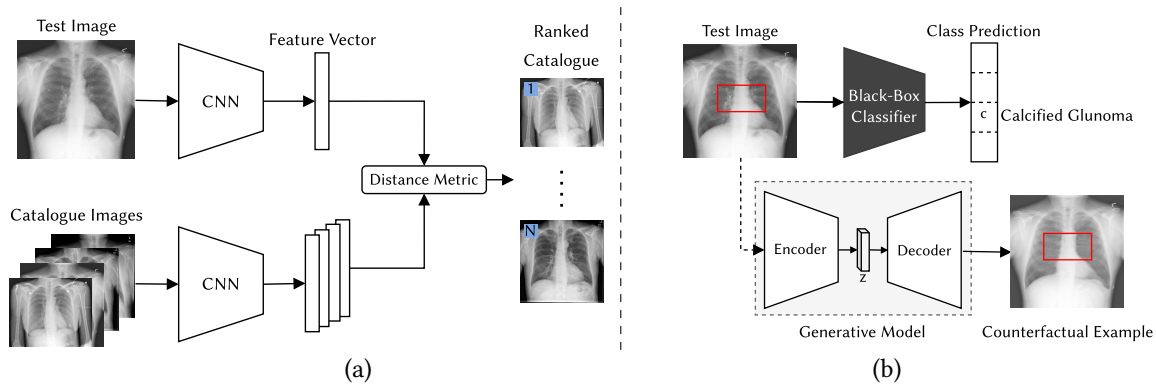


**Fig. 6. (a) Explanation by Case-Based Reasoning.** The feature vector corresponding to the input image is compared against the feature vectors of the images in the catalogue using a distance metric, such as L2 distance. Finally, the images are retrieved from the catalogue ranked by their similarity to the input image. **(b) Explanation by Counterfactual Examples.** To explain the prediction made by a classifier, the input image is modified in a controlled way, typically by using a generative model (e.g., GAN) to shift the original class, i.e., from normal to abnormal or vice-versa. Thus, the counterfactual example intends to explain the prediction by showing that the image was classified as “abnormal” because it is not “normal”, as perceived by the absence of tissue inflammation (white spots) in the generated counterfactual example.

The work of Schutte et al. [111] constituted a new approach in the way of interpreting the predictions made by deep learning models by using generative models to produce a sequence of images depicting the evolution of a pathology. Through the sequence of images produced, a human can understand which biomarkers triggered the prediction made by the model. Concretely, the proposed method aims to identify the optimal direction in latent space to produce a series of synthetic images with minor modifications leading to different model predictions. By observing these modified synthetic versions of the original image, it is expectable that a human can perceive the features that caused the model prediction. Experimental results on two medical image datasets showed that the proposed approach allows visualizing where the most relevant features are localized and how they contributed to the model prediction by analyzing the generated images. Moreover, this generative approach may be helpful for the identification of new biomarkers.

Kim et al. [54] proposed the Counterfactual Generative Network (CGN), which is able to generate counterfactual images to explain the predictions of a pneumonia classifier from chest X-ray images. To guide the CGN towards the generation of contrastive images from query image, the prediction of the classification network was manipulated to shift the original class to the negative class. The subtraction of the counterfactual image from the input image allows the generation of attribution maps evidencing the most relevant regions to the prediction.

In the same fashion, Singla et al. [121] used a conditional Generative Adversarial Network (cGAN) to produce a set of counterfactual images with changed posterior probability to explain the class predictions of a chest X-ray classifier. Additionally, the context from semantic segmentation and object detection was incorporated into the loss function to preserve subtle information about the medical images in the generated counterfactual images. The validity of the generated counterfactual explanations was assessed through the use of three evaluation metrics, namely 1) Fréchet Instance Distance score to evaluate the visual quality of the counterfactual images, 2) Counterfactual Validity score to quantify the class floppiness of the counterfactual images, and 3) Foreign Object Preservation score to assess the presence of unique properties of patients in the generated explanations. Furthermore, clinical measurements, namely, cardiothoracic ratio and costophrenic recess, were adopted to demonstrate the utility of the explanations in terms of the clinical context.

**5.3.3 Prototypes.** Although most of the reviewed works attempted to explain a black-box model, Rudin [105] argued that the best option is to use inherently interpretable models instead of relying on post-hoc explanations. In her work, Rudin refer to two works that proposed different approaches to design interpretable CNN architectures. The first work was done by Chen et al. [19], in which they incorporate a prototype layer at the end of the network [13; 19], named ProtoPNet, for bird species recognition. The rationale behind this approach is that different parts of the image act as class-representative prototypes during training. When a new image needs to be evaluated in the testing phase, the network finds the most similar prototypes to the parts of the test image. The final class prediction is based on a score computed with the similarities between the prototypes. Figure 7 illustrates the general pipeline for deriving a class prediction from the similarity score between different parts of the input image and a set of learned prototypes.

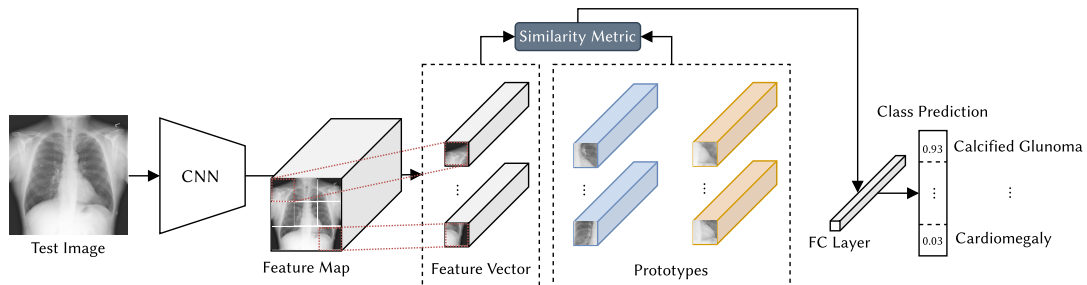


**Fig. 7. Explanation by prototypes.** During the model training, a set of prototypes are learned to visually represent a certain class (represented with blue and orange colours in the figure). In the test phase, the features extracted from the test image are compared with a set of prototypes using a similarity metric, such as cosine similarity. Then, the final class prediction is based on the similarity scores computed between the prototypes and the different parts of the input image.

Based on ProtoPNet, Donnelly et al. [28] introduced the Deformable ProtoPNet. This prototypical case-based interpretable neural network provided spatially flexible deformable prototypes, i.e., prototypes that can change their relative position to detect semantically similar parts of an input image.

Despite the significance of ProtoPNet, Hoffmann et al. [44] investigated its shortcomings, and proved that ProtoPNet could be susceptible to adversarial and compression noise, and thus compromise the inner interpretability of the model. Although these limitations were not significant in the bird recognition problem, the picture changes in high-stake applications, such as the healthcare domain, where the lack of robustness can have severe implications.

Regarding the applicability of these inherently interpretable networks to medical imaging, Kim et al. [53] proposed an interpretable diagnosis framework, dubbed XProtoNet, for chest radiography to learn disease representative features within a dynamic area, using an occurrence map. Contrary to ProtoPNet, in XProtoNet the prototypes are class-representative and completely dynamic in terms of area, which is particularly important for accommodating the high variability in size of discriminative regions of medical images. To produce an appropriate occurrence map, the authors introduced two regularization terms. The L1 loss forced the occurrence area to be small enough to avoid covering irrelevant regions, and transformation loss approximate each occurrence map with a transformed version via an affine transformation that did not change the relative location of a disease pattern. The experiments on NIH Chest X-ray dataset [142] confirmed that the XProtoNet surpasses the state-of-the-art models in diagnosing chest diseases from X-ray images. Later, Singh et al. [118] introduced an interpretable deep learning model, named Generalized Prototypical Part Network (Gen-ProtoPNet), for detecting Covid-19 from X-ray images. Gen-ProtoPNet was inspired in the original ProtoPNet [19] and the NP-ProtoPNet [119]. Unlike ProtoPNet and NP-ProtoPNet that use L2 distance to calculate the similarity between prototypes, Gen-ProtoPNet used a generalized version of the L2 distance, allowing the use of prototypical parts of any dimension, i.e., squared and rectangular spatial dimensions. Furthermore, the experiments on two Covid-19 chest X-ray datasets [24; 140] confirmed that using prototypical parts of spatial dimensions bigger than  $1 \times 1$  improves performance of the model, specifically when using the VGG-16 model as the feature extractor.

*Discussion.* Relying on example-based strategies perhaps might be a more trustworthy option since the retrieved examples are plausible and tend to contain similar findings to the input query image. However, the performance of the example-based systems can be compromised if a significant number of examples per class is unavailable. This assumption is also valid in the case of prototype-based approaches, where performance depends directly on the diversity and amount of class-representative prototypes. Regarding the counterfactual explanations, it is desirable to discover credible causal structures to create ground-truth explanations to improve further the modelling of the interventions made over the images [121].

#### 5.4 Explanation by Concepts

The rationale behind concept-based learning approaches is using human-specified concepts as an intermediate step to derive the final predictions. This idea was previously used in the works of Kumar et al. [59] and Lampert et al. [60], with specific applications in few-shot learning approaches. In [60], the proposed model first estimated a set of attributes and then used those predicted attributes to infer the final predictions. These types of model architectures were dubbed Concept Bottleneck Models (CBM) in the work of Koh et al. [56]. In simple terms, these models relied on an encoder-decoder paradigm, where the encoder is responsible for predicting the concepts given the raw input image, and the decoder leverages the predicted concepts by the encoder to make the final predictions. The encoder is typically a CNN model with a bottleneck layer inserted after the last convolutional layer, while the decoder can be a multi-layer perceptron to map the concepts to the final predictions. This typical pipeline is illustrated in Figure 8. The idea of CBMs can be applied to any model just by inserting the bottleneck layer after the final convolutional layer. However, the main disadvantage of these methods is that annotated concepts are required. Koh et al. provided a systematic study on different ways to learn CBMs. Among the considered setup models, they concluded that the joint training is the preferred approach, which minimizes the weighted sum considering the classification loss and concept loss. The authors also stated that it is possible to

intervene in the concept predictions to change the final output. The question arises to what extent it is feasible to revisit, for example, 100 concepts and perceive which concept would be modified to make the correct prediction.

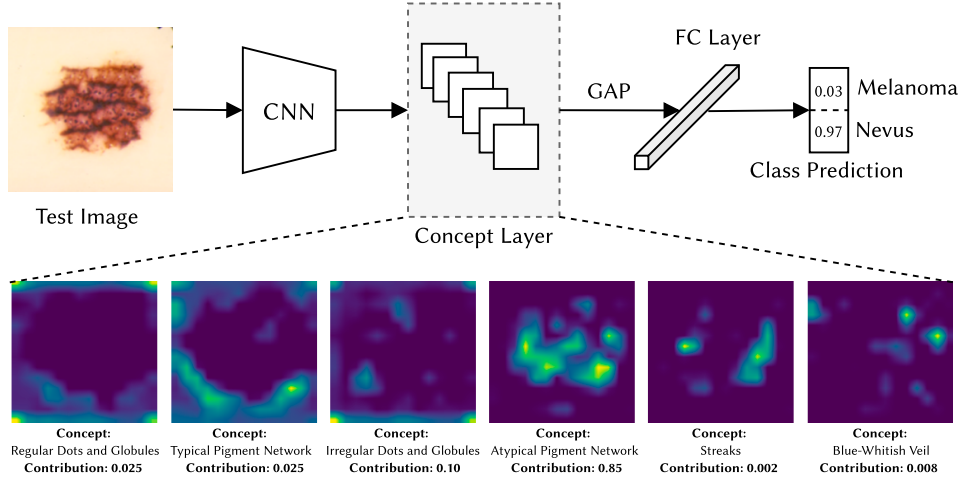


**Fig. 8. Explanation by Concepts.** In the first phase, the concept layer is trained to predict the concepts associated with the input image. Then, given a test image, the model first predicts the concepts presented in the image. The concepts are then mapped to a fully connected layer to make the final predictions. Furthermore, it is possible to produce visualizations of the filters of the concept layer that highlight the relevant regions for each concept. Additionally, the contribution of each concept to the final prediction is obtained to perceive which concepts had more influence on the final decision.

A different approach was introduced by Chen et al. [20] where they proposed the Concept Whitening (CW), a module that is inserted into a neural network, and that can replace the Batch Normalization layer so that each point in the latent space has an interpretation in terms of known concepts. In a similar line of research, Wickramanayake et al. [144] proposed the Comprehensive CNN (CCNN) to explain the model decisions in terms of word phrases. To this end, the authors added a concept layer to the CNN architecture to learn the associations between visual features and word phrases. The classification decision is then sustained by the concepts learned and their contribution to the prediction. The learning of meaningful concepts was achieved due to the concept uniqueness loss, which enforces each concept to correspond to only one word phrase. On the other hand, the mapping consistency loss preserves the distance between the visual features and the word representation in a joint embedding space. The experimental results showed that CCNN achieved higher performance than other interpretable classifiers, namely ProtoPNet, while achieving comparable performance with black-box classifiers.

Ghorbani et al. [36] introduced ACE, which can automatically identify a set of high-level concepts in an unsupervised way. In a first phase, each image is segmented in multiple resolutions using the SLIC [1] algorithm. Then, the segments are clustered by its similarity according to the euclidian distance, which is measured in the latent space. Each group of segments represents a different concept, labelled as pseudo-concepts. Lastly, to retain only the important concepts in each group, the TCAV [52] importance score was computed. The work of Fang et al. [31] built on the rationale of the ACE. The authors proposed the Visual Concept Mining (VCM) method to explain the decisions of an infectious keratitis classifier based on human-interpretable concepts. VCM comprehends two stages: (i) first, the proposed Potential Concept Generator module is responsible for identifying relevant concepts based on the segmentation of image patches according to the relevant regions highlighted on the produced saliency maps. Then, (ii) the visual concept extractor module learns the similarity and diversity

among the segmented image parts and groups them according to the DeepCluster [18] algorithm. The authors of VCM claimed that the concepts learned by their method were coherent with the medical annotations whilst being more diverse for the different classes, contrary to the ACE, which provides too broad concepts.

*Discussion.* Although concept-based explanation methods are under-explored in medical imaging, they constitute a promising way of providing human-understandable explanations. The main advantage of these methods is that they are interpretable by design since the final predictions are derived from the learned concepts. However, the dependency on manual annotation of these concepts is the major limitation in concept-learning approaches. Recently, to overcome the annotation-dependency of the concepts, proposed methods built on unsupervised techniques to discover a set of pseudo-concepts related to the input image.

## 5.5 Other Approaches

Differently from the above-discussed approaches, some authors have investigated alternative strategies to confer interpretability to the models, including Bayesian Neural Networks (BNN) to quantify the uncertainty associated with the model prediction or using adversarial training to improve the quality of the generated explanations.

**5.5.1 Bayesian Approaches.** Despite the success of CNN architectures, it is infeasible to quantify their uncertainty, given the deterministic nature associated with the internal parameters. Furthermore, CNNs are likely to overestimate the data when it is biased. In order to address these problems, Thiagarajan et al. [128] proposed the use of Bayesian CNNs (BCNN), which allow for the uncertainty estimation associated with the predictions. In particular, the uncertainty associated with the predictions of an Invasive Ductal Carcinoma (IDC) classifier on breast histopathology images was quantified. The examples characterized by a high value of uncertainty were projected into a lower-dimensional space to facilitate data visualization. Thus, the test data were represented in a 3-dimensional space using the t-SNE [134] technique, divided by degree of uncertainty (epistemic uncertainty). Furthermore, the uncertainty allowed determining which examples require human evaluation, which constitutes an interesting approach in the case of problems in the medical imaging domain. Similarly, Billah and Javed [14] relied on BCNNs to quantify the uncertainty associated to the predictions of a classifier model for the diagnosis of blood cancer. Recently, Gour and Jain [38] proposed the UA-ConvNet, an uncertainty-aware CNN to detect COVID-19 from chest X-ray images and provide an estimation of the model uncertainty. For this, they used Monte Carlo dropout [33] to obtain a probability distribution of the model prediction.

**5.5.2 Adversarial Training.** In adversarial training, examples of the training set are augmented with adversarial perturbations at each training loop. Thus, adversarially trained models are considered robust models since they are more resistant when faced with perturbed examples than standard trained models [10].

The first attempt on using adversarial training to improve interpretability in a medical imaging diagnosis task was made by Margelou et al. [82]. They explored the use of adversarial training to improve the interpretability of CNNs, mainly when applied to diagnosing skin cancer. Specifically, the trained model was retrained from scratch using adversarial training with the PGD adversary attack [78]. The experiments on the dermatology dataset HAM10000 [132] showed that saliency maps on the robust model are significantly sharper and visually coherent than those obtained from the standard trained model.

However, further research is needed since adversarial training is under-explored in medical imaging interpretability. Specifically, applying the above-referred findings to other datasets and network architectures becomes necessary to perceive the generalization capability of the methods. Furthermore, as stated by the authors in [82], the proposed method is not ready to be deployed in real-world scenarios due to the sensitivity of saliency methods to training noise, leading to capture artifacts (e.g., dark regions and irrelevant medical regions). Therefore, it is crucial to understand the limitations of adversarial training to improve interpretability in medical imaging diagnosis tasks.

Table 4. Summary of the XAI methods categorized by algorithm used, image modality and dataset. The spaces marked with a “-” mean that explanation is only provided through text sentences.

Method	Year	Algorithm	Modality	Dataset
Zhang et al. [152]	2017	Attention-based	Microscopic Images	BCIDR
Jing et al. [48]	2017	Attention-based	X-ray	IU Chest X-ray, PEIR Gross
Rajpurkar et al. [99]	2018	CAM	X-ray	ChestX-ray8
Wang et al. [143]	2018	Saliency maps	X-ray	IU Chest X-ray, ChestX-ray14
Gale et al. [34]	2018	SmoothGrad	X-ray	Pelvic X-ray
Li et al. [66]	2018	REINFORCE	X-ray	IU Chest X-ray, CX-CHR (private)
Mallhi et al. [81]	2019	LIME	Endoscopy	Red Lesion Endoscopy
Young et al. [149]	2019	KernelSHAP	Dermoscopy	HAM10000
Eitel et al. [30]	2019	Occlusion	MRI	ADNI Initiative
Sayres et al. [109]	2019	Integrated Gradients	Fundus Images	Private
Barata et al. [11]	2019	CAM	Dermoscopy	ISIC 2017, ISIC 2018
Tschandl et al. [131]	2019	CBIR	Dermoscopy	EDRA, ISIC 2017, Private Dataset
Sun et al. [126]	2019	CNN-RNN	Mammography	Inbreast
Lee et al. [64]	2019	Saliency maps	Mammography	CBIS-DDSM
Lamy et al. [61]	2019	CBR	Mammography	BCW, Mammographic Mass, Breast Cancer
Singh et al. [120]	2019	Stacked LSTM	X-ray	IU Chest X-ray
Yin et al. [148]	2019	t-SNE	X-ray	IU Chest X-ray
Liu et al. [72]	2019	Attention maps	X-ray	IU Chest X-ray, MIMIC-CXR
Windish et al. [146]	2020	Grad-CAM	MRI	IXI, Glioblastoma
Magesh et al. [79]	2020	LIME	DataScan	PPMI
Lin et al. [68]	2020	Grad-CAM, Guided Grad-CAM	X-ray	COVIDDx
Lopatina et al. [73]	2020	DeepLIFT	MRI	Private
Graziani et al. [39]	2020	TCAV	Microscopic Images	Camelyon16, Camelyon17
Margeletti et al. [82]	2020	Gradient, Integrated Gradient	Microscopic Images	HAM10000
Rio-Torto et al. [102]	2020	LRP, DeconvNet, Guided Grad-CAM	Microscopic Images	NIH-NCI Cervical Cancer
Fang et al. [31]	2020	Concept-based	Microscopic Images	Infectious Keratitis Dataset
Chen et al. [21]	2020	Multi-Head Attention	X-ray	IU Chest X-ray, MIMIC-CXR
Silva et al. [115]	2020	CBIR, Saliency Map	X-ray	CheXpert
Punn et al. [98]	2021	LIME	X-ray	COVID-19 Dataset
Wang et al. [141]	2021	SHAP	Dermoscopy	HAM10000
Billah and Javed [14]	2021	BCNN	Microscopy Images	ALL-IDB
Barata et al. [12]	2021	CBIR	Dermoscopy	ISIC 2018
Thiagarajan et al. [128]	2021	t-SNE	Microscopic Images	Breast Histopathology
Barnett et al. [13]	2021	Prototype Activation Map	Mammography	Mammography Private Dataset
Kim et al. [54]	2021	Counterfactual Examples	X-ray	Chest X-ray 14, VinDr-CXR
Singla et al. [121]	2021	Counterfactual Examples	X-ray	MIMIC-CXR
Schutte et al. [111]	2021	Grad-CAM	X-ray/Microscopy Images	Osteoarthritis X-ray, Camelyon16
Kim et al. [53]	2021	Saliency maps	X-ray	NIH chest X-ray14
Singh et al. [118]	2021	Prototype Activation Maps	X-ray	CORD-19
Lucieri et al. [74]	2022	TCAV	Dermoscopy	ISIC 2019, Derm7pt, PH2, Skin1L2
Hu et al. [46]	2022	CBIR	X-ray/Dermoscopy	COVIDDx, ISIC 2019
Gour and Jain [38]	2022	Monte Carlo dropout	X-ray	COVID19CXr

## 6 EVALUATION METRICS

Depending on the type of explanation modality (visual or textual), there are different ways to assess the quality of the generated explanations. We divide the evaluation metrics used in the literature into two categories: (i) evaluation metrics to assess the quality of visual explanations; and (ii) evaluation metrics for measuring the quality of textual explanations.

### 6.1 Evaluating the Quality of Visual Explanations

Evaluating the quality of model explanations remains an active area of research. A common approach for evaluating the model interpretability, specifically when applied to the medical domain, is to request an expert opinion from the clinicians and radiologists. However, this evaluation approach is time-consuming and depends on the level of experience of the clinicians [34; 133].

Therefore, there has been attempts to propose evaluation metrics capable of objectively assess the quality of the explanations. Samek et al. [108] were precursors in contributing to the question of how to objectively evaluate the quality of heatmaps by introducing the area over the Most Relevant First (MoRF) perturbation curve (AOPC) measure. This measure is based on a region perturbation strategy that iteratively removes information from some regions of the input image according to its relevance to the class, allowing to perceive the performance decay of the model. The conducted experiments showed that a large AOPC value denotes high model sensitivity to the perturbations, indicating that the heatmap is actually informative.

Inspired by the work in [108], Petsiuk et al. [96] proposed two causal metrics, namely deletion and insertion, to evaluate the produced explanations for a black-box model. The deletion metric measures the degradation of the class probability, as important pixels of the image, derived from the saliency map, are removed. On the other hand, the insertion metric intends to measure the increase of the class probability, as pixels are inserted based on the generated saliency map.

Later, Hooker et al. [45] argued that the modification-based metrics introduced by Petsiuk et al. [96] might not capture the actual reasoning behind the model's degradation since this degradation could be due to artefacts introduced by the values used to replace the removed pixels. Thus, the authors proposed the RemOve And Retrain (ROAR) to evaluate interpretability methods by verifying how the accuracy of a retrained model degrades as important features are removed. The most important features are removed in certain fractions in each data sample with a fixed uninformative value for each interpretability method. The main drawback of this metric is the required retraining of the model, which is computationally expensive.

Recently, Rio-Torto et al. [102] proposed the POMPOM (Percentage of Meaningful Pixels Outside the Mask) metric, which report the number of meaningful pixels outside the region of interest in relation to the total number of pixels, to evaluate the quality of a given explanation. Similarly, Barnett et al. [13] introduced the Activation Precision evaluation metric, to quantify the proportion of relevant information from the “relevant region” used to classify the mass margin regarding the radiologist annotations. Despite the relevance of both metrics, they require manual annotations of the masks, which is time-consuming and may be difficult to obtain for some medical image datasets.

In spite of the valuable contribution of these proposed evaluation metrics, we believe that a new evaluation method for model interpretability could be developed with the aid of the Bayesian Neural Networks (BNN) characteristics. Since the weights of the BNN follow a probability distribution, we can sample models from the posterior distribution and generate  $N$  explanations for a given example [17]. Then, using intersection or union operations over those generated explanations seems to be an interesting direction to estimate whether most of the explanations highlight the same Region Of Interest (ROI).

## 6.2 Evaluating the Quality of Textual Explanations

In this category, the metrics are used to measure the quality of the generated text, and are originated from generic NLP tasks. The most widely used metrics in the reviewed papers were BLEU [93], ROUGE-L [67], METEOR [63] and CIDEr [137].

BLEU (Bilingual Evaluation Understudy) score is the most common evaluation metric in NLP. In simple terms, it compares  $n$ -gram matches between the generated sentence (also known as candidate sentence) and the ground-truth sentence (also known as reference sentence), expressed in modified precision<sup>1</sup> for each  $n$ -gram. The BLEU metric has  $N$  variations (BLEU-N), typically  $N \in \{1, 2, 3, 4\}$ , with respect to the considered  $n$ -grams. The value of BLEU score ranges from 0 to 1, which means that the closer to 1, the better the translation. Formally, BLEU score is computed according to the following formulation:

$$\text{BLEU} = \text{BP} \cdot \exp \sum_{n=1}^N w_n \log p_n, \quad (1)$$

where  $p_n$  is the modified precision for  $n$ -gram,  $w_n$  is a weight, ranging from 0 and 1, and  $\sum_{n=1}^N w_n = 1$ , i.e., if  $N = 4$ ,  $w_n = 1/N$ , and BP is the brevity penalty that penalizes short generated sentences, denoted as:

$$\text{BP} = \begin{cases} 1 & \text{if } c > r \\ \exp(1 - \frac{1}{c}) & \text{if } c \leq r \end{cases}, \quad (2)$$

where  $c$  is the length of candidate translation, and  $r$  is the reference corpus length.

The ROUGE (Recall-Oriented Understudy for Gisting Evaluation) metric is actually a set of metrics. We focus on the ROUGE-L variant as it was the prevalent metric in the most of the reviewed methods. ROUGE-L measures the Longest Common Subsequence (LCS) between the generated sentence and the ground-truth sentence both in terms of precision and recall. This means that if both sentences share a long sub-sentence, the similarity between the two sentences is expected to be high. The final value of ROUGE-L is given in F1 score, as formally described below (Eq. 3):

$$\text{ROUGE-L}_{F1} = 2 \cdot \frac{\text{Precision} \cdot \text{Recall}}{\text{Precision} + \text{Recall}}, \quad (3)$$

where  $\text{Precision} = \frac{\text{LCS}(c,r)}{m}$  and  $\text{Recall} = \frac{\text{LCS}(c,r)}{n}$ , with  $\text{LCS}(c,r)$  denoting the Longest Common Subsequence between the candidate sentence ( $c$ ) and the reference sentence ( $r$ ),  $m$  is the number of  $n$ -grams in the reference sentence, and  $n$  the number of  $n$ -grams in the candidate sentence.

Differently from the two above-discussed metrics, METEOR (Metric for Evaluation of Translation with Explicit Ordering) gives attention to the position of the words in the sentence by including a chunk penalty that weights the final score.

$$\text{METEOR} = F_{\text{mean}} \cdot (1 - \text{Penalty}) \quad (4)$$

where  $\text{Penalty} = 0.5 \cdot (\frac{m}{n})$ , where  $m$  is the number of chunks and  $n$  is the total number of unigram matches, and  $F_{\text{mean}} = \frac{10PR}{R+9P}$ .

Alternatively, CIDEr (Consensus-Based Image Description Evaluation) is an evaluation metric that uses the Term Frequency Inverse Document Frequency (TF-IDF) [103] for weighting each  $n$ -gram. The intuition behind CIDEr is that  $n$ -grams that frequently appear in the reference sentences are less likely to be informative, and

<sup>1</sup>Takes into consideration the maximum frequency of each n-gram in the reference sentence (clipped count). The modified precision is then calculated by summing the clipped counts of the candidate sentence divided by the total number of candidate n-grams.

hence they have a lower weight using the IDF term.  $CIDEr_n$ ,  $n = \{1, 2, 3, 4\}$ , is the average cosine similarity between the candidate sentence and the reference sentences, considering both precision and recall.

TF-IDF weighting  $g_k(s_{ij})$  for each  $n$ -gram  $w_k$  is computed as follows:

$$g_k(s_{ij}) = \frac{h_k(s_{ij})}{\sum_{w_l \in \omega} h_l(s_{ij})} \log\left(\frac{|I|}{\sum_{I_p \in I} h_k(s_{pq})}\right) \min(1, \sum_q h_k(s_{pq})), \quad (5)$$

where  $h_k(s_{ij})$  is the number of times an  $n$ -gram occurs in a reference sentence  $s_{ij}$ , and  $h_k(c_i)$  for the candidate sentence  $c_i$ ,  $\omega$  is the vocabulary of all  $n$ -grams, and  $I$  is the set of all images.

$$CIDEr_n(c_i, S_i) = \frac{1}{m} \sum_j \frac{g^n(c_i) \cdot g^n(s_{ij})}{\|g^n(c_i)\| \|g^n(s_{ij})\|}. \quad (6)$$

The final CIDEr score is the weighted average of  $CIDEr_n$ :

$$CIDEr(c_i, S_i) = \sum_{n=1}^N w_n CIDEr_n(c_i, S_i), \quad (7)$$

where  $w_n = 1/N$ ,  $N = 4$ .

## 7 PERFORMANCE COMPARISON

In the previous sections, several methods were selected and discussed concerning their categorization. At the end of the review, an important question arises: “*What is the best approach?*”. However, in many cases, there is no trivial answer. Most methods adopted different evaluation metrics making performance comparison with other competing methods unfeasible. In order to find common ground for a fair comparison of the methods, only those methods that considered the same dataset for evaluation purposes were selected. As presented in table 5, IU Chest X-ray [27] is the most used dataset among the reviewed methods. As such, we verified whether the methods that were evaluated on the IU Chest X-ray [27] used the same evaluation metrics. We find out that these methods (Jing et al. [48], Singh et al. [120], HRNN [148], HRGR-Agent [66], TieNet<sup>1</sup> [143], Liu et al. [72], and R2Gen [21]) have adopted the same evaluation metrics, namely BLEU score, ROUGE, METEOR, and CIDEr. Additionally, 3 out of the 7 methods were evaluated on a different dataset, the MIMIC-CXR [49], and used the same evaluation metrics. In this way, a comparison of the performance between these seven methods was carried out. Table 5 presents the results in terms of the above-referred NLP evaluation metrics for each of the selected methods.

### 7.1 Results Discussion

It is worth noticing that all the presented results in table 5 were taken from the original paper of each method, except for the TieNet [143] method, whose results were taken from the work of Liu et al. [72], since in the original paper the authors only provide results in ChestX-ray14 using BLEU, METEOR, and ROUGE-L.

Regarding the methods that considered the “findings+impression” section from the radiology report to generate the free-text report, and as evidenced by the results in table 5, the model proposed by Jing et al. [48] achieved the best results in all evaluation metrics by a considerable margin except for the CIDEr metric, where the method of Singh et al. reached the highest value (0.36). The co-attention mechanism adopted by Jing et al. can explain the method’s superior performance compared with its competitors. Moreover, Jing et al. relied on a hierarchical LSTM model that performs better in generating long text reports, whereas Singh et al. [120] only used a stack of LSTMs.

As for methods that only take into account the “findings” section, the R2Gen [21] model excels in all evaluation metrics. The superior performance obtained by R2Gen can be explained due to the use of memory modules

Table 5. Performance comparison among the selected methods that generates textual explanations for explaining model decisions. The mid rule inserted after HRNN [148] row separates the methods by which report sections are generated by each model: “*findings + impression*” or only “*findings*”. Spaces marked with a “-” mean no value is available for the respective metric.<sup>1</sup> Results were taken from the work of Liu et al. [72].

<b>Model</b>	<b>BLEU-1</b>	<b>BLEU-2</b>	<b>BLEU-3</b>	<b>BLEU-4</b>	<b>ROUGE-L</b>	<b>METEOR</b>	<b>CIDEr</b>
<i>IU Chest X-Ray</i>							
Jing et al. [48]	<b>0.517</b>	<b>0.386</b>	<b>0.306</b>	<b>0.247</b>	<b>0.447</b>	<b>0.217</b>	0.327
Singh et al. [120]	0.374	0.224	0.153	0.110	0.308	0.164	<b>0.360</b>
HRNN [148]	0.445	0.292	0.201	0.154	0.344	0.175	0.342
HRGR-Agent [66]	0.438	0.298	0.208	0.151	0.322	-	0.343
TieNet <sup>1</sup> [143]	0.330	0.194	0.124	0.081	0.311	-	1.334
Liu et al. [72]	0.369	0.246	0.171	0.115	0.359	-	<b>1.490</b>
R2Gen [21]	<b>0.470</b>	<b>0.304</b>	<b>0.219</b>	<b>0.165</b>	<b>0.371</b>	<b>0.187</b>	-
<i>MIMIC-CXR</i>							
R2Gen [21]	<b>0.353</b>	0.218	0.145	0.103	0.277	0.142	-
TieNet <sup>1</sup> [143]	0.332	0.212	0.142	0.095	0.296	-	1.004
Liu et al. [72]	0.352	<b>0.223</b>	<b>0.153</b>	<b>0.104</b>	<b>0.307</b>	-	<b>1.153</b>

coupled with the decoder of the Transformer. These modules retain textual patterns and assist the Transformer’s decoder to generate radiology reports containing relevant information.

With respect to the results obtained for the MIMIC-CXR dataset, R2Gen is partially toppled by the model of Liu et al. [48], which performs better in generating groups of words ( $n$ -grams  $> 1$ ), however by a minimal margin. The fine-tuning procedure adopted by the Liu et al. [48], using reinforcement learning via CIDEr score to ensure more coherent report generation, can explain the superior performance, indicating that this strategy works well in large-scale datasets, namely the MIMIC-CXR dataset.

## 8 DISCUSSION AND FUTURE WORK

Although XAI is a relatively recent research field, its constant growth is undeniable, with applications in many areas, particularly in the medical domain. However, despite the advances and the efforts made toward developing interpretable deep learning-based models for medical imaging, there are open issues that require more research and advances in this growing field. This section identifies open challenges in the literature and potential research paths to further improve the trustworthiness of provided explanations and foster the adoption of deep learning-based systems into clinical routine.

Among the reviewed literature, we can conclude that the go-to method for model interpretation in medical imaging is producing saliency maps, using classical techniques, such as Grad-CAM, Integrated Gradients, or LRP. However, as evidenced by some authors, saliency maps can be unreliable and fragile [2; 105], as they often highlight irrelevant regions in the images. In addition, it is frequent that very similar explanations are given for different classes, and often none of them are useful explanations [105]. Moreover, different end-users could have different backgrounds and preferences at interpreting the explanation, which can generate some contradictory opinions. This fostered the use of textual explanations, which are preferred over visual explanations by some authors [34] since they are inherently understandable by humans [138]. Since then, methods that generate textual descriptions for explaining a prediction and multimodal methods that combine visual and textual explanations

have emerged. However, generating free-text reports is deemed a challenging task since the radiologist reports are technically structured, and the most used language models based on RNNs have some limitations in generating long texts, as stated by Pascanu et al. [94].

Therefore, another research direction was providing explanations by examples, which is directly linked to how humans try to explain something by showing other examples related to the subject intended to be explained. This way, some example-based approaches have emerged with promising results that were even comparable to the performance of standard classifiers. These example-based methods include CBR approaches, prototype-based and concept-based strategies. Recently, Schutte et al. [111] introduced a disruptive approach that strives to generate synthetic examples to explain a model decision, as discussed in section 5.5. The possible limitations of using example-based methods are related to the availability of a considerable amount of data covering all the classes in a balanced way, without forgetting the sensibility of these methods to adversarial attacks, even though this can be prevented by using adversarial training [82].

On the other hand, the development of inherently interpretable models has been a line of research with promising results in the medical imaging domain. Although these methods remain largely unexplored in medical imaging, future research will undoubtedly be devoted to develop inherently interpretable models. These models have the primary benefit of providing their own explanations, which contributes to their transparency and fidelity, increasing the chances of being adopted into the clinical routine.

Alternatively, other methods have emerged as candidates for explaining the decision of a model. The adoption of Bayesian Neural Networks to estimate or quantify the uncertainty regarding the model predictions might be an interesting option, although few works attempted to prove its effectiveness.

Future research in medical image interpretability can also include the use of vision transformers (ViTs) [29]. According to [83], vision transformers proved to be comparable with CNN in terms of performance (accuracy) in the medical classification tasks. Furthermore, ViTs have the benefit of providing a type of built-in saliency maps that are used to better understand the model's decisions.

Regarding medical image datasets, existing publicly available datasets for medical image captioning are limited in number and there is need to generate more large size datasets. Moreover, most of the existing datasets has focused only on few anatomical parts of body, such as chest, while ignoring other important parts like breast and brain [8].

## 8.1 Challenges and Future Research Trends

Despite the rapid pace of advances in the medical imaging and deep learning, there are problems that remain without a definitive solution.

*Small datasets.* Collecting a medical imaging dataset involves multiple entities and background bureaucracies. Nevertheless, the main issue is related to the availability of the physicians in annotating a vast amount of data, that is time-consuming and costly. To surpass these constraints, distinct data augmentation techniques have emerged as an alternative for collecting new data. Recently, Wickramanayake et al. [145] proposed the BRACE framework to augment the dataset based on concept-based explanations from model decisions, which can help to discover the samples in the under-represented regions in the training set. Furthermore, Wickramanayake et al. introduced a utility function to select the images in the under-representation regions and concepts that caused the misclassification. The images with a high utility score are selected to incorporate the training set. On the other hand, the use of generative approaches to perform data augmentation in a controlled way might be an interesting research direction.

*Insufficient labelled data.* Although most works rely on the supervised learning paradigm, it is often not the best choice when working in the medical domain, since the process of label annotation is time-consuming and

costly for large-scale datasets, especially in domains such as digital pathology where the manual annotation is subject to inter- and intra-observer variability [150]. Transfer learning was adopted in most works to address these issues, but this technique is not completely effective in the medical domain, since the original models were trained in images belonging to standard object detection datasets (e.g., ImageNet), which do not share the same patterns of medical imagery. This way, Self-Supervised Learning (SSL) has emerged to tackle these challenges, allowing the network to learn visual meaningful feature representations without the need of annotated data [23]. Besides its effectiveness in dealing with scarce labelled data, it confers robustness to the model, rendering it more resistant to adversarial attacks. In medical imaging, the use of SSL seems to be a promising research direction due to the characteristics of medical datasets. Furthermore, contrastive learning approaches have achieved impressive results, due to the contrastive loss that forces the network to learn high-level features that occur in images across multiple views, which are created through the use of geometric transformation such as random cropping, color distortion, gaussian blur. For a comprehensive overview of the state-of-the-art of SSL with a particular focus on medical domain we refer the reader to [23].

*Qualitative assessment of the explanations.* The automated evaluation of the explanations provided by interpretability methods remains an open challenge. As previously discussed in section 6.1, the most adopted method for evaluating the explanations in the context of the medical domain is to resort to the clinician’s expertise. However, considering variability in experts opinions [130], this strategy is particularly biased and subjective. On the other hand, the existing strategies for objectively measuring the quality of visual explanations are still dependent on manual annotations of relevant regions [102], or iterative model retraining (ROAR [45]). For these reasons, we believe that the design of objective metrics for assessing the quality of the model explanations will be one of the important research rends on the topic of XAI.

*Report generation in medical imaging.* Text-based explanations are usually obtained using RNN-based approaches through the generation of words forming a sentence. Nevertheless, RNN-based approaches have some limitations in generating long text reports [94]. Consequently, the use of Transformers for the automatic generation of radiology reports was adopted in an attempt to overcome the limitations of traditional RNNs, namely the problem of vanishing gradients. The self-attention mechanism of the Transformer architecture allows for the learning of contextual relationships between the words that constitute the sequence. In addition, Transformer-based networks can be trained faster than traditional RNNs as they allow for simultaneous processing of sequential data. On the other hand, using concept-based approaches as a transition bridge between free-text report generation and concept-based explanations may be an exciting future research direction. Instead of trying to generate free-text reports, which is challenging, having a set of concepts that are sufficient to describe the phenomenon depicted in the image can support clinicians in writing a complete report.

## 9 CONCLUSIONS

This paper reviewed the advances on explainable deep learning applied to medical diagnosis. First we introduced a comparative analysis between the existing surveys on the topic, where the major conclusions and weakness of the each were highlighted. Then, the most prominent XAI methods were briefly described to provide the readers with fundamental concepts of the field, necessary to the discussion of the recent advances on the medical imaging domain. Additionally, several frameworks that implement XAI methods were presented and a brief discussion of the existing medical imaging datasets was drawn. After this, we comprehensively reviewed the works focused on explaining the decision process of deep learning applied to medical imaging. The works were group according to the explanation modality comprising explanations by feature attribution, explanations by text, explanation by examples and explanations by concepts. Contrary to other surveys on the topic, we focused this review on inherently interpretable models over post-hoc approaches, which has been recently considered future

research direction on deep learning interpretability. The discussion of the adopted evaluation metrics used in the literature was also carried out, where we described the existing metrics to assess the quality of visual explanations and the commonly NLP metrics to evaluate the quality of the generated textual explanations. Additionally, a comparison of the performance of a set of prominent XAI methods was performed based on the dataset used and the evaluation metrics adopted. Finally, the discussion and future outlook in XAI for medical diagnosis were addressed where we identified open challenges in the literature and potential research avenues to improve the trustworthiness of provided explanations and foment the adoption of deep learning-based systems into clinical routine. To conclude, we believe that this survey will be helpful to the XAI community, particularly to the medical imaging field, as an entry point to guide the research and the future advances in the topic of XAI.

## REFERENCES

- [1] Radhakrishna Achanta, Appu Shaji, Kevin Smith, Aurelien Lucchi, Pascal Fua, and Sabine Süsstrunk. 2012. SLIC Superpixels Compared to State-of-the-Art Superpixel Methods. *IEEE Transactions on Pattern Analysis and Machine Intelligence* 34, 11 (2012), 2274–2282.
- [2] Julius Adebayo, Justin Gilmer, Michael Muelly, Ian Goodfellow, Moritz Hardt, and Been Kim. 2018. Sanity Checks for Saliency Maps. *Advances in Neural Information Processing Systems* 31 (2018).
- [3] Ceyhun Burak Akgül, Daniel L Rubin, Sandy Napel, Christopher F Beaulieu, Hayit Greenspan, and Burak Acar. 2011. Content-Based Image Retrieval in Radiology: Current Status and Future Directions. *Journal of Digital Imaging* 24, 2 (2011), 208–222.
- [4] Maximilian Alber, Sebastian Lapuschkin, Philipp Seegerer, Miriam Hägle, Kristof T. Schütt, Grégoire Montavon, Wojciech Samek, Klaus-Robert Müller, Sven Dähne, and Pieter-Jan Kindermans. 2019. iNNvestigate Neural Networks! *Journal of Machine Learning Research* 20, 93 (2019), 1–8.
- [5] Stefano Allegretti, Federico Bolelli, Federico Pollastri, Sabrina Longhitano, Giovanni Pellacani, and Costantino Grana. 2021. Supporting Skin Lesion Diagnosis with Content-Based Image Retrieval. In *Proceedings of the IEEE International Conference on Pattern Recognition (ICPR)*. 8053–8060.
- [6] Marco Ancona, Enea Ceolini, Cengiz Öztireli, and Markus Gross. 2018. Towards better understanding of gradient-based attribution methods for Deep Neural Networks. In *International Conference on Learning Representations (ICLR)*.
- [7] Samuel G Armato III, Geoffrey McLennan, Luc Bidaut, Michael F McNitt-Gray, Charles Meyer, Anthony P Reeves, Binsheng Zhao, Denise R Aberle, Claudia I Henschke, Eric A Hoffman, et al. 2011. The Lung Image Database Consortium (LIDC) and Image Database Resource Initiative (IDRI): a completed reference database of lung nodules on CT scans. *Medical Physics* 38, 2 (2011), 915–931.
- [8] Hareem Ayesha, Sajid Iqbal, Mehreen Tariq, Muhammad Abrar, Muhammad Sanaullah, Ishaq Abbas, Amjad Rehman, Muhammad Farooq Khan Niazi, and Shafiq Hussain. 2021. Automatic medical image interpretation: State of the art and future directions. *Pattern Recognition* 114 (2021), 107856.
- [9] Sebastian Bach, Alexander Binder, Grégoire Montavon, Frederick Klauschen, Klaus-Robert Müller, and Wojciech Samek. 2015. On Pixel-Wise Explanations for Non-Linear Classifier Decisions by Layer-Wise Relevance Propagation. *PLoS ONE* 10, 7 (2015), e0130140.
- [10] Tao Bai, Jinqi Luo, Jun Zhao, Bihan Wen, and Qian Wang. 2021. Recent Advances in Adversarial Training for Adversarial Robustness. In *Proceedings of the International Joint Conference on Artificial Intelligence (IJCAI)*. 4312–4321.
- [11] Catarina Barata, Jorge S Marques, and M Emre Celebi. 2019. Deep Attention Model for the Hierarchical Diagnosis of Skin Lesions. In *Proceedings of the IEEE Conference on Computer Vision and Pattern Recognition Workshops (CVPRW)*. 2757–2765.
- [12] Catarina Barata and Carlos Santiago. 2021. Improving the Explainability of Skin Cancer Diagnosis Using CBIR. In *Proceedings of the International Conference on Medical Image Computing and Computer-Assisted Intervention (MICCAI)*. 550–559.
- [13] Alina Jade Barnett, Fides Regina Schwartz, Chaofan Tao, Chaofan Chen, Yinhao Ren, Joseph Y Lo, and Cynthia Rudin. 2021. Interpretable Mammographic Image Classification using Case-Based Reasoning and Deep Learning. *arXiv preprint arXiv:2107.05605* (2021).
- [14] Mohammad Ehtasham Billah and Farrukh Javed. 2022. Bayesian Convolutional Neural Network-based Models for Diagnosis of Blood Cancer. *Applied Artificial Intelligence* (2022), 1–22.
- [15] Hamidreza Bolhasani, Elham Amjadi, Maryam Tabatabaeian, and Somayeh Jafarali Jassbi. 2020. A histopathological image dataset for grading breast invasive ductal carcinomas. *Informatics in Medicine Unlocked* 19 (2020), 100341.
- [16] Aurelia Bustos, Antonio Pertusa, Jose-Maria Salinas, and Maria de la Iglesia-Vayá. 2020. PadChest: A large chest x-ray image dataset with multi-label annotated reports. *Medical Image Analysis* 66 (2020), 101797.
- [17] Kirill Bykov, Marina M-C Höhne, Adelaida Creosteanu, Klaus-Robert Müller, Frederick Klauschen, Shinichi Nakajima, and Marius Kloft. 2021. Explaining Bayesian Neural Networks. *arXiv preprint arXiv:2108.10346* (2021).
- [18] Mathilde Caron, Piotr Bojanowski, Armand Joulin, and Matthijs Douze. 2018. Deep Clustering for Unsupervised Learning of Visual Features. In *Proceedings of the European Conference on Computer Vision (ECCV)*. 132–149.

- [19] Chaofan Chen, Oscar Li, Chaofan Tao, Alina Jade Barnett, Jonathan Su, and Cynthia Rudin. 2019. This Looks Like That: Deep Learning for Interpretable Image Recognition. In *Proceedings of the International Conference of Neural Information Processing Systems (NIPS)*.
- [20] Zhi Chen, Yijie Bei, and Cynthia Rudin. 2020. Concept Whitening for Interpretable Image Recognition. *Nature Machine Intelligence* 2, 12 (2020), 772–782.
- [21] Zhihong Chen, Yan Song, Tsung-Hui Chang, and Xiang Wan. 2020. Generating Radiology Reports via Memory-driven Transformer. In *Proceedings of the Conference on Empirical Methods in Natural Language Processing (EMNLP)*. 1439–1449.
- [22] Deepak Roy Chittajallu, Bo Dong, Paul Tunison, Roddy Collins, Katerina Wells, James Fleshman, Ganesh Sankaranarayanan, Steven Schwitzberg, Lora Cavuto, and Andinet Enquobahrie. 2019. XAI-CBIR: Explainable AI System for Content based Retrieval of Video Frames from Minimally Invasive Surgery Videos. In *Proceedings of the IEEE International Symposium on Biomedical Imaging (ISBI)*. 66–69.
- [23] Alexander Chowdhury, Jacob Rosenthal, Jonathan Waring, and Renato Umeton. 2021. Applying Self-Supervised Learning to Medicine: Review of the State of the Art and Medical Implementations. *Informatics* 8, 3 (2021), 59.
- [24] Joseph Paul Cohen, Paul Morrison, and Lan Dao. 2020. COVID-19 Image Data Collection. *arXiv* 2003.11597 (2020). <https://github.com/ieee8023/covid-chestxray-dataset>
- [25] Jesus M Darias, Belén Diaz-Agudo, and Juan A Recio-Garcia. 2021. A Systematic Review on Model-agnostic XAI Libraries. (2021).
- [26] Sergio de Faria, Jose Filipe, Pedro Pereira, Luis Tavora, Pedro Assuncao, Miguel Santos, Rui Fonseca-Pinto, Felicidade Santiago, Victoria Dominguez, and Martinha Henrique. 2019. Light Field Image Dataset of Skin Lesions. In *Proceedings of the International Conference of the IEEE Engineering in Medicine and Biology Society (EMBC)*. 3905–3908.
- [27] Dina Demner-Fushman, Marc D Kohli, Marc B Rosenman, Sonya E Shooshan, Larita Rodriguez, Sameer Antani, George R Thoma, and Clement J McDonald. 2016. Preparing a collection of radiology examinations for distribution and retrieval. *Journal of the American Medical Informatics Association* 23, 2 (2016), 304–310.
- [28] Jon Donnelly, Alina Jade Barnett, and Chaofan Chen. 2021. Deformable ProtoPNet: An Interpretable Image Classifier Using Deformable Prototypes. *arXiv preprint arXiv:2111.15000* (2021).
- [29] Alexey Dosovitskiy, Lucas Beyer, Alexander Kolesnikov, Dirk Weissenborn, Xiaohua Zhai, Thomas Unterthiner, Mostafa Dehghani, Matthias Minderer, Georg Heigold, Sylvain Gelly, Jakob Uszkoreit, and Neil Houlsby. 2021. An Image is Worth 16x16 Words: Transformers for Image Recognition at Scale. In *Proceedings of the International Conference on Learning Representations (ICLR)*.
- [30] Fabian Eitel and Kerstin Ritter for the Alzheimer’s Disease Neuroimaging Initiative (ADNI). 2019. Testing the Robustness of Attribution Methods for Convolutional Neural Networks in MRI-Based Alzheimer’s Disease Classification. In *Interpretability of Machine Intelligence in Medical Image Computing and Multimodal Learning for Clinical Decision Support (IMIMIC)*. 3–11.
- [31] Zhengqing Fang, Kun Kuang, Yuxiao Lin, Fei Wu, and Yu-Feng Yao. 2020. Concept-based Explanation for Fine-grained Images and Its Application in Infectious Keratitis Classification. In *Proceedings of the ACM International Conference on Multimedia*. 700–708.
- [32] Ruth Fong, Mandela Patrick, and Andrea Vedaldi. 2019. Understanding Deep Networks via Extremal Perturbations and Smooth Masks. In *Proceedings of the IEEE/CVF International Conference on Computer Vision (ICCV)*. 2950–2958.
- [33] Yarin Gal and Zoubin Ghahramani. 2016. Dropout as a Bayesian Approximation: Representing Model Uncertainty in Deep Learning. In *Proceedings of the International Conference on Machine Learning (ICML)*. 1050–1059.
- [34] William Gale, Luke Oakden-Rayner, Gustavo Carneiro, Andrew P Bradley, and Lyle J Palmer. 2019. Producing Radiologist-Quality Reports for Interpretable Deep Learning. In *Proceedings of the IEEE International Symposium on Biomedical Imaging (ISBI)*. 1275–1279.
- [35] Amirata Ghorbani, Abubakar Abid, and James Zou. 2019. Interpretation of Neural Networks is Fragile. In *Proceedings of the AAAI Conference on Artificial Intelligence*, Vol. 33. 3681–3688.
- [36] Amirata Ghorbani, James Wexler, James Y Zou, and Been Kim. 2019. Towards Automatic Concept-Based Explanations. In *Advances in Neural Information Processing Systems*, Vol. 32.
- [37] Bryce Goodman and Seth Flaxman. 2017. European Union Regulations on Algorithmic Decision-Making and a “Right to Explanation”. *AI Magazine* 38, 3 (2017), 50–57.
- [38] Mahesh Gour and Sweta Jain. 2022. Uncertainty-aware convolutional neural network for COVID-19 X-ray images classification. *Computers in Biology and Medicine* 140 (2022), 105047.
- [39] Mara Graziani, Vincent Andrearczyk, Stéphane Marchand-Maillet, and Henning Müller. 2020. Concept attribution: Explaining CNN decisions to physicians. *Computers in Biology and Medicine* 123 (2020), 103865.
- [40] Mehmet A Gulum, Christopher M Trombley, and Mehmed Kantardzic. 2021. A Review of Explainable Deep Learning Cancer Detection Models in Medical Imaging. *Applied Sciences* 11, 10 (2021), 4573.
- [41] David Gunning and David Aha. 2019. DARPA’s Explainable Artificial Intelligence (XAI) Program. *AI Magazine* 40, 2 (2019), 44–58.
- [42] Tarun Gupta, Libin Kutty, Ritu Gahir, Nnamdi Ukwu, Sayantan Polley, and Marcus Thiel. 2021. IRTEX: Image Retrieval with Textual Explanations. In *Proceedings of the IEEE International Conference on Human-Machine Systems (ICHMS)*. 1–4.
- [43] David M. Hansell, Alexander A. Bankier, Heber MacMahon, Theresa C. McLoud, Nestor L. Müller, and Jacques Remy. 2008. Fleischner Society: Glossary of Terms for Thoracic Imaging. *Radiology* 246, 3 (2008), 697–722.

- [44] Adrian Hoffmann, Claudio Fanconi, Rahul Rade, and Jonas Kohler. 2021. This Looks Like That... Does it? Shortcomings of Latent Space Prototype Interpretability in Deep Networks. In *ICML Workshop on Theoretic Foundation, Criticism, and Application Trend of Explainable AI*.
- [45] Sara Hooker, Dumitru Erhan, Pieter-Jan Kindermans, and Been Kim. 2019. A Benchmark for Interpretability Methods in Deep Neural Networks. In *Advances in Neural Information Processing Systems*, Vol. 32. 9737–9748.
- [46] Brian Hu, Bhavan Vasu, and Anthony Hoogs. 2022. X-MIR: EXplainable Medical Image Retrieval. In *Proceedings of the IEEE/CVF Winter Conference on Applications of Computer Vision (WACV)*. 440–450.
- [47] Jeremy Irvin, Pranav Rajpurkar, Michael Ko, Yifan Yu, Silviana Ciurea-Ilcus, Chris Chute, Henrik Marklund, Behzad Haghgoo, Robyn Ball, Katie Shpanskaya, et al. 2019. CheXpert: A Large Chest Radiograph Dataset with Uncertainty Labels and Expert Comparison. In *Proceedings of the AAAI Conference on Artificial Intelligence*, Vol. 33. 590–597.
- [48] Baoyu Jing, Pengtao Xie, and Eric Xing. 2018. On the Automatic Generation of Medical Imaging Reports. In *Proceedings of the 56th Annual Meeting of the Association for Computational Linguistics (ACL)*.
- [49] Alistair EW Johnson, Tom J Pollard, Seth J Berkowitz, Nathaniel R Greenbaum, Matthew P Lungren, Chih-ying Deng, Roger G Mark, and Steven Horng. 2019. MIMIC-CXR, a de-identified publicly available database of chest radiographs with free-text reports. *Scientific Data* 6, 1 (2019), 1–8.
- [50] Jeremy Kawahara, Sara Daneshvar, Giuseppe Argenziano, and Ghassan Hamarneh. 2019. Seven-Point Checklist and Skin Lesion Classification Using Multitask Multimodal Neural Nets. *IEEE Journal of Biomedical and Health Informatics* 23, 2 (2019), 538–546.
- [51] Oisin J. F. Keenan, George Holland, Julian F. Maempel, John F. Keating, and Chloe E. H. Scott. 2020. Correlations between radiological classification systems and confirmed cartilage loss in severe knee osteoarthritis. *The Bone & Joint Journal* 102-B, 3 (2020), 301–309.
- [52] Been Kim, Martin Wattenberg, Justin Gilmer, Carrie J. Cai, James Wexler, Fernanda B. Viégas, and Rory Sayres. 2018. Interpretability Beyond Feature Attribution: Quantitative Testing with Concept Activation Vectors (TCAV). In *Proceedings of the International Conference on Machine Learning (ICML)*. 2668–2677.
- [53] Eunji Kim, Siwon Kim, Minji Seo, and Sungroh Yoon. 2021. XProtoNet: Diagnosis in Chest Radiography with Global and Local Explanations. In *Proceedings of the IEEE/CVF Conference on Computer Vision and Pattern Recognition (CVPR)*. 15719–15728.
- [54] Junho Kim, Minsu Kim, and Yong Man Ro. 2021. Interpretation of Lesional Detection via Counterfactual Generation. In *Proceedings of the IEEE International Conference on Image Processing (ICIP)*. 96–100.
- [55] Pieter-Jan Kindermans, Kristof T Schütt, Maximilian Alber, Klaus-Robert Müller, Dumitru Erhan, Been Kim, and Sven Dähne. 2018. Learning how to explain neural networks: PatternNet and PatternAttribution. In *International Conference on Learning Representations (ICML)*.
- [56] Pang Wei Koh, Thao Nguyen, Yew Siang Tang, Stephen Mussmann, Emma Pierson, Been Kim, and Percy Liang. 2020. Concept Bottleneck Models. In *Proceedings of the International Conference on Machine Learning (ICML)*. 5338–5348.
- [57] Kokhlikyanet. 2019. Pytorch Captum. [Online]. Accessed January, 21 2021. Available: <https://github.com/pytorch/captum>.
- [58] Alex Krizhevsky, Ilya Sutskever, and Geoffrey E Hinton. 2012. ImageNet Classification with Deep Convolutional Neural Networks. *Advances in Neural Information Processing Systems (NIPS)* 25 (2012).
- [59] Neeraj Kumar, Alexander C. Berg, Peter N. Belhumeur, and Shree K. Nayar. 2009. Attribute and Simile Classifiers for Face Verification. In *Proceedings of the IEEE International Conference on Computer Vision (CVPR)*. 365–372.
- [60] Christoph H Lampert, Hannes Nickisch, and Stefan Harmeling. 2009. Learning to Detect Unseen Object Classes by Between-class Attribute Transfer. In *Proceedings of the IEEE Conference on Computer Vision and Pattern Recognition (CVPR)*. 951–958.
- [61] Jean-Baptiste Lamy, Boomadevi Sekar, Gilles Guezenec, Jacques Bouaud, and Brigitte Séroussi. 2019. Explainable artificial intelligence for breast cancer: A visual case-based reasoning approach. *Artificial Intelligence in Medicine* 94 (2019), 42–53.
- [62] Sebastian Lapuschkin, Alexander Binder, Grégoire Montavon, Klaus-Robert Müller, and Wojciech Samek. 2016. The LRP Toolbox for Artificial Neural Networks. *Journal of Machine Learning Research* 17, 114 (2016), 1–5.
- [63] Alon Lavie and Abhaya Agarwal. 2007. METEOR: An Automatic Metric for MT Evaluation with High Levels of Correlation with Human Judgments. In *Proceedings of the Workshop on Statistical Machine Translation*. 228–231.
- [64] Hyebin Lee, Seong Tae Kim, and Yong Man Ro. 2019. Generation of Multimodal Justification Using Visual Word Constraint Model for Explainable Computer-Aided Diagnosis. In *Interpretability of Machine Intelligence in Medical Image Computing and Multimodal Learning for Clinical Decision Support*. 21–29.
- [65] Rebecca Sawyer Lee, Francisco Gimenez, Assaf Hoogi, Kanae Kawai Miyake, Mia Gorovoy, and Daniel L Rubin. 2017. A curated mammography data set for use in computer-aided detection and diagnosis research. *Scientific Data* 4, 1 (2017), 1–9.
- [66] Christy Y Li, Xiaodan Liang, Zhitong Hu, and Eric P Xing. 2018. Hybrid Retrieval-Generation Reinforced Agent for Medical Image Report Generation. In *Proceedings of the International Conference on Neural Information Processing Systems (NIPS)*. 1537–1547.
- [67] Chin-Yew Lin. 2004. ROUGE: A Package for Automatic Evaluation of Summaries. In *Text Summarization Branches Out*. 74–81.
- [68] Tsung-Chieh Lin and Hsi-Chieh Lee. 2020. Covid-19 Chest Radiography Images Analysis Based on Integration of Image Preprocess, Guided Grad-CAM, Machine Learning and Risk Management. In *Proceedings of the International Conference on Medical and Health Informatics (ICMHI)*. 281–288.

- [69] Zachary C Lipton. 2017. The Doctor Just Won't Accept That! *arXiv preprint arXiv:1711.08037* (2017).
- [70] Geert Litjens, Peter Bandi, Babak Ehteshami Bejnordi, Oscar Geessink, Maschenka Balkenhol, Peter Bult, Altuna Halilovic, Meyke HermSEN, Rob van de Loo, and Rob Vogels. 2018. 1399 H&E-stained sentinel lymph node sections of breast cancer patients: the CAMELYON dataset. *GigaScience* 7, 6 (2018).
- [71] Geert Litjens, Thijs Kooi, Babak Ehteshami Bejnordi, Arnaud Arindra Adiyoso Setio, Francesco Ciompi, Mohsen Ghafoorian, Jeroen Awm Van Der Laak, Bram Van Ginneken, and Clara I Sánchez. 2017. A Survey on Deep Learning in Medical Image Analysis. *Medical Image Analysis* 42 (2017), 60–88.
- [72] Guanxiong Liu, Tzu-Ming Harry Hsu, Matthew McDermott, Willie Boag, Wei-Hung Weng, Peter Szolovits, and Marzyeh Ghassemi. 2019. Clinically Accurate Chest X-Ray Report Generation. In *Machine Learning for Healthcare Conference*. 249–269.
- [73] Alina Lopatina, Stefan Ropele, Renat Sibgatulin, Jürgen R Reichenbach, and Daniel Güllmar. 2020. Investigation of Deep-Learning-Driven Identification of Multiple Sclerosis Patients Based on Susceptibility-Weighted Images Using Relevance Analysis. *Frontiers in Neuroscience* (2020), 1356.
- [74] Adriano Lucieri, Muhammad Naseer Bajwa, Stephan Alexander Braun, Muhammad Imran Malik, Andreas Dengel, and Sheraz Ahmed. 2022. ExAID: A Multimodal Explanation Framework for Computer-Aided Diagnosis of Skin Lesions. *Computer Methods and Programs in Biomedicine* (2022), 106620.
- [75] Adriano Lucieri, Muhammad Naseer Bajwa, Andreas Dengel, and Sheraz Ahmed. 2020. Explaining AI-based Decision Support Systems using Concept Localization Maps. In *Proceedings of the International Conference on Neural Information Processing*. 185–193.
- [76] Scott M Lundberg, Gabriel G Erion, and Su-In Lee. 2018. Consistent Individualized Feature Attribution for Tree Ensembles. *arXiv preprint arXiv:1802.03888* (2018).
- [77] Scott M Lundberg and Su-In Lee. 2017. A Unified Approach to Interpreting Model Predictions. In *Proceedings of the International Conference on Neural Information Processing Systems (NIPS)*. 4768–4777.
- [78] Aleksander Madry, Aleksandar Makelov, Ludwig Schmidt, Dimitris Tsipras, and Adrian Vladu. 2018. Towards Deep Learning Models Resistant to Adversarial Attacks. In *Proceedings of the International Conference on Learning Representations (ICLR)*.
- [79] Pavan Rajkumar Magesh, Richard Delwin Myloth, and Rijo Jackson Tom. 2020. An Explainable Machine Learning Model for Early Detection of Parkinson's Disease using LIME on DaTscan Imagery. *Computers in Biology and Medicine* 126 (2020), 104041.
- [80] Anna Majkowska, Sid Mittal, David F Steiner, Joshua J Reicher, Scott Mayer McKinney, Gavin E Duggan, Krish Eswaran, Po-Hsuan Cameron Chen, Yun Liu, Sreenivasa Raju Kalidindi, et al. 2020. Chest Radiograph Interpretation with Deep Learning Models: Assessment with Radiologist-adjudicated Reference Standards and Population-adjusted Evaluation. *Radiology* 294, 2 (2020), 421–431.
- [81] Avleen Malhi, Timotheus Kampik, Husanbir Pannu, Manik Madhikermi, and Kary Främling. 2019. Explaining Machine Learning-Based Classifications of In-Vivo Gastral Images. In *Digital Image Computing: Techniques and Applications (DICTA)*. 1–7.
- [82] Andrei Margeloiu, Nikola Simidjevski, Mateja Jamnik, and Adrian Weller. 2020. Improving Interpretability in Medical Imaging Diagnosis using Adversarial Training. In *Medical Imaging Meets NeurIPS Workshop*.
- [83] Christos Matsoukas, Johan Fredin Haslum, Magnus Söderberg, and Kevin Smith. 2021. Is it Time to Replace CNNs with Transformers for Medical Images? *arXiv preprint arXiv:2108.09038* (2021).
- [84] Teresa Mendonça, Pedro Ferreira, Jorge Marques, André Marcal, and Jorge Rozeira. 2013. PH 2-A dermoscopic image database for research and benchmarking. In *Proceedings of the International Conference of the IEEE Engineering in Medicine and Biology Society (EMBS)*. 5437–5440.
- [85] Pablo Messina, Pablo Pino, Denis Parra, Alvaro Soto, Cecilia Besa, Sergio Uribe, Cristian Tejos, Claudia Prieto, Daniel Capurro, et al. 2021. A Survey on Deep Learning and Explainability for Automatic Image-based Medical Report Generation. *Comput. Surveys* (2021).
- [86] Christoph Molnar. 2022. Interpretable Machine Learning: A Guide for Making Black Box Models Explainable. Available: <https://christophm.github.io/interpretable-ml-book>.
- [87] Grégoire Montavon, Sebastian Lapuschkin, Alexander Binder, Wojciech Samek, and Klaus-Robert Müller. 2017. Explaining NonLinear Classification Decisions with Deep Taylor Decomposition. *Pattern Recognition* 65 (2017), 211–222.
- [88] Johanna D Moore and William R Swartout. 1988. Explanation in Expert Systems: A Survey. *University of Southern California* (1988).
- [89] Inês C Moreira, Igor Amaral, Inês Domingues, António Cardoso, Maria Joao Cardoso, and Jaime S Cardoso. 2012. INbreast: Toward a Full-field Digital Mammographic Database. *Academic Radiology* 19, 2 (2012), 236–248.
- [90] M Nevitt, D Felson, and Gayle Lester. 2006. The Osteoarthritis Initiative. *Protocol for the Cohort Study* 1 (2006).
- [91] Ha Nguyen, Khanh Lam, Linh Le, Hieu Pham, Dat Tran, Dung Nguyen, Dung Le, Chi Pham, Hang Tong, Diep Dinh, Cuong Do, Luu Doan, Cuong Nguyen, Binh Nguyen, Que Nguyen, Au Hoang, Hien Phan, Anh Nguyen, Phuong Ho, Dat Ngo, Nghia Nguyen, Nhan Nguyen, Minh Dao, and Van Vu. 2020. VinDr-CXR: An Open Dataset of Chest X-rays with Radiologist's Annotations. *arXiv preprint arXiv:2012.15029* (2020).
- [92] Hieu T. Nguyen, Hieu H. Pham, Nghia T. Nguyen, Ha Q. Nguyen, Thang Q. Huynh, Minh Dao, and Van Vu. 2021. VinDr-SpineXR: A Deep Learning Framework for Spinal Lesions Detection and Classification from Radiographs. In *Proceedings of the International Conference on Medical Image Computing and Computer Assisted Intervention (MICCAI)*. 291–301.

- [93] Kishore Papineni, Salim Roukos, Todd Ward, and Wei-Jing Zhu. 2002. BLEU: a Method for Automatic Evaluation of Machine Translation. In *Proceedings of the Annual Meeting of the Association for Computational Linguistics (ACL)*. 311–318.
- [94] Razvan Pascanu, Tomas Mikolov, and Yoshua Bengio. 2013. On the difficulty of training Recurrent Neural Networks. In *Proceedings of the International Conference on Machine Learning (ICML)*. 1310–1318.
- [95] Obioma Pelka, Sven Koitka, Johannes Rückert, Felix Nensa, et al. 2018. Radiology Objects in COntext (ROCO): A Multimodal Image Dataset. In *Intravascular Imaging and Computer Assisted Stenting and Large-Scale Annotation of Biomedical Data and Expert Label Synthesis*. 180–189.
- [96] Vitali Petsiuk, Abir Das, and Kate Saenko. 2018. RISE: Randomized Input Sampling for Explanation of Black-box Models. In *British Machine Vision Conference (BMVC)*.
- [97] Milda Pocevičiūtė, Gabriel Eilertsen, and Claes Lundström. 2020. Survey of XAI in Digital Pathology. In *Artificial Intelligence and Machine Learning for Digital Pathology: State-of-the-Art and Future Challenges*. 56–88.
- [98] Narinder Singh Punn and Sonali Agarwal. 2021. Automated diagnosis of COVID-19 with limited posteroanterior chest X-ray images using fine-tuned deep neural networks. *Applied Intelligence* 51, 5 (2021), 2689–2702.
- [99] Pranav Rajpurkar, Jeremy Irvin, Robyn L Ball, Kaylie Zhu, Brandon Yang, Hershel Mehta, Tony Duan, Daisy Ding, Aarti Bagul, et al. 2018. Deep learning for chest radiograph diagnosis: A retrospective comparison of the CheXNeXt algorithm to practicing radiologists. *PLoS medicine* 15, 11 (2018).
- [100] Asia Rehman, Muheet Ahmed Butt, and Majid Zaman. 2021. A Survey of Medical Image Analysis Using Deep Learning Approaches. In *Proceedings of the IEEE International Conference on Computing Methodologies and Communication (ICCMC)*. 1334–1342.
- [101] Marco Tulio Ribeiro, Sameer Singh, and Carlos Guestrin. 2016. "Why Should I Trust You?": Explaining the Predictions of Any Classifier. In *Proceedings of the ACM SIGKDD International Conference on Knowledge Discovery and Data Mining*. 1135–1144.
- [102] Isabel Rio-Torto, Kelwin Fernandes, and Luís Teixeira. 2020. Understanding the decisions of CNNs: An in-model approach. *Pattern Recognition Letters* 133 (2020), 373–380.
- [103] Stephen Robertson. 2004. Understanding Inverse Document Frequency: on Theoretical Arguments for IDF. *Journal of Documentation* 60 (2004), 503–520.
- [104] Veronica Rotemberg, Nicholas Kurtansky, Brigid Betz-Stablein, Liam Caffery, Emmanouil Chousakos, Noel Codella, Marc Combalia, Stephen Dusza, Pascale Guitera, David Gutman, et al. 2021. A Patient-Centric Dataset of Images and Metadata for Identifying Melanomas Using Clinical Context. *Scientific Data* 8, 1 (2021), 1–8.
- [105] Cynthia Rudin. 2019. Stop Explaining Black Box Machine Learning Models for High Stakes Decisions and Use Interpretable Models Instead. *Nature Machine Intelligence* 1, 5 (2019), 206–215.
- [106] Mahya Sadeghi, Parmit K Chilana, and M Stella Atkins. 2018. How Users Perceive Content-based Image Retrieval for Identifying Skin Images. In *Understanding and Interpreting Machine Learning in Medical Image Computing Applications*. 141–148.
- [107] Zohaib Salahuddin, Henry C. Woodruff, Avishhek Chatterjee, and Philippe Lambin. 2022. Transparency of Deep Neural Networks for Medical Image Analysis: A Review of Interpretability Methods. *Computers in Biology and Medicine* 140 (2022), 105111.
- [108] Wojciech Samek, Alexander Binder, Grégoire Montavon, Sebastian Lapuschkin, and Klaus-Robert Müller. 2016. Evaluating the Visualization of What a Deep Neural Network Has Learned. *IEEE Transactions on Neural Networks and Learning Systems* 28, 11 (2016), 2660–2673.
- [109] Rory Sayres, Ankur Taly, Ehsan Rahimy, Katy Blumer, David Coz, Naama Hammel, Jonathan Krause, Arunachalam Narayanaswamy, Zahra Rastegar, Derek Wu, et al. 2019. Using a Deep Learning Algorithm and Integrated Gradients Explanation to Assist Grading for Diabetic Retinopathy. *Ophthalmology* 126, 4 (2019), 552–564.
- [110] Thomas Schlegl, Sebastian M Waldstein, Wolf-Dieter Vogl, Ursula Schmidt-Erfurth, and Georg Langs. 2015. Predicting Semantic Descriptions from Medical Images with Convolutional Neural Networks. In *Proceedings of the International Conference on Information Processing in Medical Imaging (IPMI)*. 437–448.
- [111] Kathryn Schutte, Olivier Moindrot, Paul Hérent, Jean-Baptiste Schiratti, and Simon Jégou. 2021. Using StyleGAN for Visual Interpretability of Deep Learning Models on Medical Images. *arXiv preprint arXiv:2101.07563* (2021).
- [112] Ramprasaath R Selvaraju, Michael Cogswell, Abhishek Das, Ramakrishna Vedantam, Devi Parikh, and Dhruv Batra. 2017. Grad-CAM: Visual Explanations from Deep Networks via Gradient-based Localization. In *Proceedings of the IEEE International Conference on Computer Vision (ICCV)*. 618–626.
- [113] L. S. Shapley. 2016. A Value for n-Person Games. In *Contributions to the Theory of Games (AM-28)*, Harold William Kuhn and Albert William Tucker (Eds.), Vol. II. 307–318.
- [114] Avanti Shrikumar, Peyton Greenside, and Anshul Kundaje. 2017. Learning Important Features Through Propagating Activation Differences. In *Proceedings of the International Conference on Machine Learning (ICML)*, Vol. 70. 3145–3153.
- [115] Wilson Silva, Alexander Poellinger, Jaime S Cardoso, and Mauricio Reyes. 2020. Interpretability-guided Content-based Medical Image Retrieval. In *Proceedings of the International Conference on Medical Image Computing and Computer-Assisted Intervention (MICCAI)*. 305–314.

- [116] Karen Simonyan, Andrea Vedaldi, and Andrew Zisserman. 2014. Deep Inside Convolutional Networks: Visualising Image Classification Models and Saliency Maps. In *Workshop at International Conference on Learning Representations (ICLR)*.
- [117] Amitojdeep Singh, Sourya Sengupta, and Vasudevan Lakshminarayanan. 2020. Explainable Deep Learning Models in Medical Image Analysis. *Journal of Imaging* 6, 6 (2020), 52.
- [118] Gurmail Singh and Kin-Choong Yow. 2021. An Interpretable Deep Learning Model For Covid-19 Detection With Chest X-ray Images. *IEEE Access* 9 (2021), 85198–85208.
- [119] Gurmail Singh and Kin-Choong Yow. 2021. These do not Look Like Those: An Interpretable Deep Learning Model for Image Recognition. *IEEE Access* 9 (2021), 41482–41493.
- [120] Sonit Singh, Sarvnaz Karimi, Kevin Ho-Shon, and Len Hamey. 2019. From Chest X-Rays to Radiology Reports: A Multimodal Machine Learning Approach. In *Digital Image Computing: Techniques and Applications (DICTA)*. 1–8.
- [121] Sumedha Singla, Brian Pollack, Stephen Wallace, and Kayhan Batmanghelich. 2021. Explaining the Black-box Smoothly - A Counterfactual Approach. *arXiv preprint arXiv:2101.04230* (2021).
- [122] Daniel Smilkov, Nikhil Thorat, Been Kim, Fernanda Viégas, and Martin Wattenberg. 2017. SmoothGrad: Removing Noise by Adding Noise. In *ICML Workshop on Visualization for Deep Learning*.
- [123] Asia Pacific Tele-Ophthalmology Society. 2019. APTOS Diabetic Retinopathy Dataset. [Online]. Accessed November, 23 2021. Available: <https://www.kaggle.com/c/aptos2019-blindness-detection/data>.
- [124] Fabio A Spanhol, Luiz S Oliveira, Caroline Petitjean, and Laurent Heutte. 2015. A Dataset for Breast Cancer Histopathological Image Classification. *IEEE Transactions on Biomedical Engineering* 63, 7 (2015), 1455–1462.
- [125] Jost Tobias Springenberg, Alexey Dosovitskiy, Thomas Brox, and Martin Riedmiller. 2014. Striving for Simplicity: The All Convolutional Net. *arXiv preprint arXiv:1412.6806* (2014).
- [126] Li Sun, Weipeng Wang, Jiyun Li, and Jingsheng Lin. 2019. Study on Medical Image Report Generation Based on Improved Encoding-Decoding Method. In *Intelligent Computing Theories and Application*. 686–696.
- [127] Mukund Sundararajan, Ankur Taly, and Qiqi Yan. 2017. Axiomatic Attribution for Deep Networks. In *Proceedings of the International Conference on Machine Learning (ICML)*. 3319–3328.
- [128] Ponkrishnan Thiagarajan, Pushkar Khairnar, and Susanta Ghosh. 2021. Explanation and Use of Uncertainty Obtained by Bayesian Neural Network Classifiers for Breast Histopathology Images. *IEEE Transactions on Medical Imaging* 41, 4 (2021), 815–825.
- [129] Erico Tjoa and Cuntai Guan. 2020. A Survey on Explainable Artificial Intelligence (XAI): Towards Medical XAI. *IEEE Transactions on Neural Networks and Learning Systems* 32, 11 (2020), 4793–4813.
- [130] Sana Tonekaboni, Shalmali Joshi, Melissa D McCradden, and Anna Goldenberg. 2019. What Clinicians Want: Contextualizing Explainable Machine Learning for Clinical End Use. In *Proceedings of the Machine Learning for Healthcare Conference*. 359–380.
- [131] Philipp Tschandl, Giuseppe Argenziano, Majid Razmara, and Jordan Yap. 2019. Diagnostic Accuracy of Content Based Dermatoscopic Image Retrieval with Deep Classification Features. *British Journal of Dermatology* 181, 1 (2019), 155–165.
- [132] Philipp Tschandl, Cliff Rosendahl, and Harald Kittler. 2018. The HAM10000 Dataset: A Large Collection of Multi-Source Dermatoscopic Images of Common Pigmented Skin Lesions. *Scientific Data* 5, 1 (2018), 1–9.
- [133] Nikos Tsiknakis, Eleftherios Trivizakis, Evangelia E Vassalou, Georgios Z Papadakis, Demetrios A Spandidos, Aristidis Tsatsakis, Jose Sánchez-García, Rafael López-González, Nikolaos Papanikolaou, Apostolos H Karantanas, et al. 2020. Interpretable artificial intelligence framework for COVID-19 screening on chest X-rays. *Experimental and Therapeutic Medicine* 20, 2 (2020), 727–735.
- [134] Laurens Van der Maaten and Geoffrey Hinton. 2008. Visualizing Data using t-SNE. *Journal of Machine Learning Research* 9, 11 (2008).
- [135] Michael Van Lent, William Fisher, and Michael Mancuso. 2004. An Explainable Artificial Intelligence System for Small-unit Tactical Behavior. In *Proceedings of the National Conference on Artificial Intelligence (AAAI)*. 900–907.
- [136] Ashish Vaswani, Noam Shazeer, Niki Parmar, Jakob Uszkoreit, Llion Jones, Aidan N Gomez, Łukasz Kaiser, and Illia Polosukhin. 2017. Attention Is All You Need. In *Advances in Neural Information Processing Systems*. 5998–6008.
- [137] Ramakrishna Vedantam, C Lawrence Zitnick, and Devi Parikh. 2015. CIDEr: Consensus-based Image Description Evaluation. In *Proceedings of the IEEE Conference on Computer Vision and Pattern Recognition (CVPR)*. 4566–4575.
- [138] Bas Velden, Hugo J Kuijf, Kenneth GA Gilhuus, and Max A Viergever. 2021. Explainable Artificial Intelligence (XAI) in Deep Learning-based Medical Image Analysis. *arXiv preprint arXiv:2107.10912* (2021).
- [139] Linda Wang, Zhong Qiu Lin, and Alexander Wong. 2020. COVID-Net: a tailored deep convolutional neural network design for detection of COVID-19 cases from chest X-ray images. *Scientific Reports* 10, 1 (2020), 1–12.
- [140] Lucy Lu Wang, Kyle Lo, Yoganand Chandrasekhar, Russell Reas, Jiangjiang Yang, Darrin Eide, Kathryn Funk, Rodney Kinney, Ziyang Liu, William Merrill, et al. 2020. CORD-19: The COVID-19 Open Research Dataset. *ArXiv* (2020).
- [141] Sutong Wang, Yunqiang Yin, Dujuan Wang, Yanzhang Wang, and Yaochu Jin. 2021. Interpretability-Based Multimodal Convolutional Neural Networks for Skin Lesion Diagnosis. *IEEE Transactions on Cybernetics* (2021).
- [142] Xiaosong Wang, Yifan Peng, Le Lu, Zhiyong Lu, Mohammad Bagheri, and Ronald Summers. 2017. ChestX-ray8: Hospital-scale Chest X-ray Database and Benchmarks on Weakly-Supervised Classification and Localization of Common Thorax Diseases. In *Proceedings of the IEEE Conference on Computer Vision and Pattern Recognition (CVPR)*. 2097–2106.

- [143] Xiaosong Wang, Yifan Peng, Le Lu, Zhiyong Lu, and Ronald Summers. 2018. TieNet: Text-Image Embedding Network for Common Thorax Disease Classification and Reporting in Chest X-rays. In *Proceedings of the IEEE Conference on Computer Vision and Pattern Recognition (CVPR)*. 9049–9058.
- [144] Sandareka Wickramanayake, Wynne Hsu, and Mong Li Lee. 2021. Comprehensible Convolutional Neural Networks via Guided Concept Learning. In *Proceedings of the IEEE International Joint Conference on Neural Networks (IJCNN)*. 1–8.
- [145] Sandareka Wickramanayake, Wynne Hsu, and Mong Li Lee. 2021. Explanation-based Data Augmentation for Image Classification. In *Advances in Neural Information Processing Systems*, Vol. 34.
- [146] Paul Windisch, Pascal Weber, Christoph Fürweger, Felix Ehret, Markus Kufeld, Daniel Zwahlen, and Alexander Muacevic. 2020. Implementation of model explainability for a basic brain tumor detection using convolutional neural networks on MRI slices. *Neuroradiology* 62, 11 (2020), 1515–1518.
- [147] Yesheng Xu, Ming Kong, Wenjia Xie, Runping Duan, Zhengqing Fang, Yuxiao Lin, Qiang Zhu, Siliang Tang, Fei Wu, and Yu-Feng Yao. 2021. Deep Sequential Feature Learning in Clinical Image Classification of Infectious Keratitis. *Engineering* 7, 7 (2021), 1002–1010.
- [148] Changchang Yin, Buyue Qian, Jishang Wei, Xiaoyu Li, Xianli Zhang, Yang Li, and Qinghua Zheng. 2019. Automatic Generation of Medical Imaging Diagnostic Report with Hierarchical Recurrent Neural Network. In *Proceedings of the IEEE International Conference on Data Mining (ICDM)*. 728–737.
- [149] Kyle Young, Gareth Booth, Becks Simpson, Reuben Dutton, and Sally Shrapnel. 2019. Deep Neural Network or Dermatologist? In *Interpretability of Machine Intelligence in Medical Image Computing and Multimodal Learning for Clinical Decision Support*. 48–55.
- [150] Hang Yu, Laurence T Yang, Qingchen Zhang, David Armstrong, and M Jamal Deen. 2021. Convolutional Neural Networks for Medical Image Analysis. *Neurocomputing* 444 (2021), 92–110.
- [151] Matthew D Zeiler and Rob Fergus. 2014. Visualizing and Understanding Convolutional Networks. In *Proceedings of the European Conference on Computer Vision (ECCV)*. 818–833.
- [152] Zizhao Zhang, Yuanpu Xie, Fuyong Xing, Mason McGough, and Lin Yang. 2017. MDNet: A Semantically and Visually Interpretable Medical Image Diagnosis Network. In *Proceedings of the IEEE Conference on Computer Vision and Pattern Recognition (CVPR)*. 6428–6436.
- [153] Bolei Zhou, Aditya Khosla, Agata Lapedriza, Aude Oliva, and Antonio Torralba. 2016. Learning Deep Features for Discriminative Localization. In *Proceedings of the IEEE Conference on Computer Vision and Pattern Recognition (CVPR)*. 2921–2929.